Evaluation of a Method to Cost-effectively Map Riparian Areas in Southern California Coastal Watersheds

Technical Report 480
February 2006

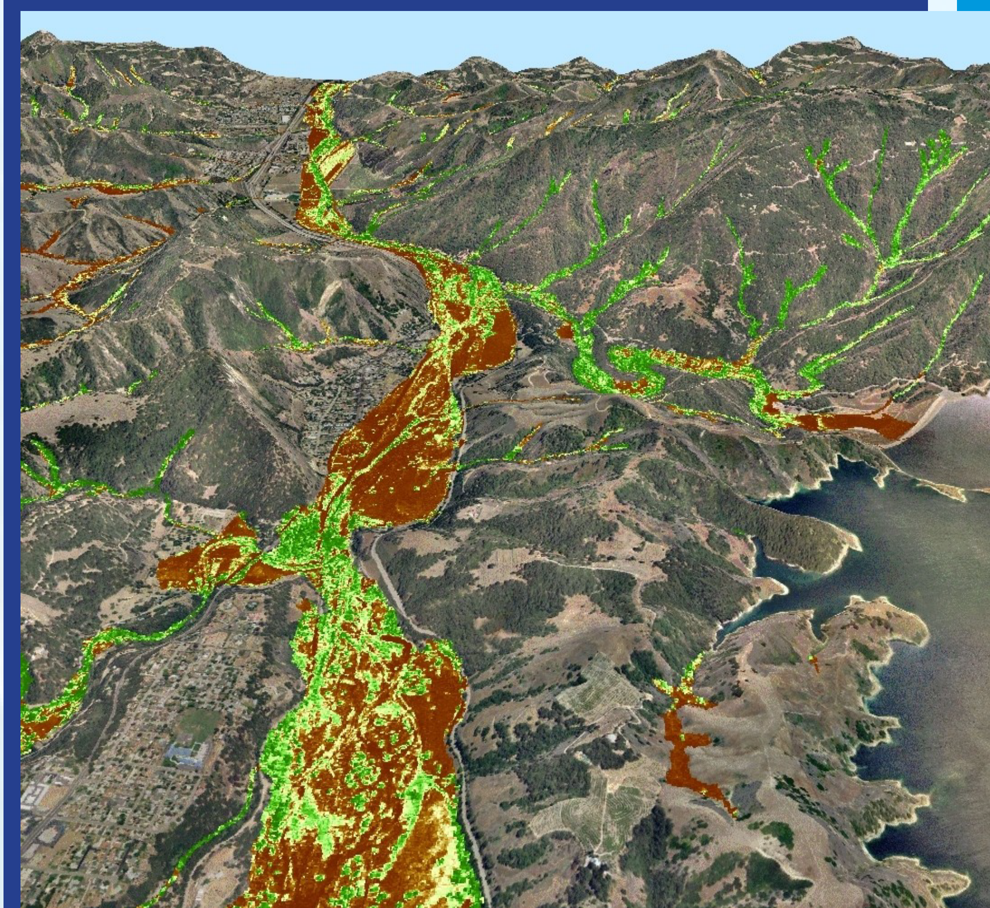

Martha Sutula
Eric Stein
Ethan Inlander

Southern California Coastal Water Research Project

EVALUATION OF A METHOD TO COST-EFFECTIVELY MAP RIPARIAN AREAS IN SOUTHERN CALIFORNIA COASTAL WATERSHEDS

Final Report to:

United States Geological Survey Gap Analysis Program
Cooperative Agreement No. 02HQAG0143

Submitted by:

Martha Sutula and Eric Stein
Southern California Coastal Water Research Project
Westminster, California

Ethan Inlander
Conception Coast Project
Santa Barbara, California

February 17, 2006

Technical Report #480

TABLE OF CONTENTS

LIST OF TABLES

LIST OF FIGURES

LIST OF ACRONYMS

AAE	Average Absolute Error
AE	Absolute Error
AVE	Average Error
C-CAP	Coastal Change Analysis Program (NOAA)
CONF	Confidence Grid
EFV	Elevation Focal Variety
LE	Less than or Equal to
MTS	Multiple-Threshold Scenario
NDVI	Normalized Difference Vegetation Index
NHD	National Hydrography Dataset (USGS)
PD	Path Distance
RMSE	Root Mean Squared Error
RZ	Riparian Zone
SSC	Subwatershed Slope Class
STS	Single-Thrshold Scenario
SWU	Sub-Watershed Unit
TAE	Total Absolute Error
TFW	Total Field Width
TRI	Topographic Ruggedness Index
VE	Valley Edge
WRP	Southern California Wetland Recovery Project

ACKNOWLEDGEMENTS

This project is dedicated to the memory of Dr. Leal A. K. Mertes, without whose teachings, trust, and inspiration the work would not have been completed. This work was funded by grants from the United States Geological Survey (USGS) GAP Analysis Program and the National Oceanic & Atmospheric Administration (NOAA) Coastal Services Center.

EXECUTIVE SUMMARY

The Southern California Coastal Water Research Project (SCCWRP), on behalf of the Southern California Wetland Recovery Project (WRP), received funding from the NOAA Coastal Services Center and the USGS GAP Analysis Program in October 2002 to conduct a pilot project, with the primary goal of providing information to better guide the selection of cost-effective riparian mapping techniques. Specifically the project objectives included: 1) development of a GIS-based methodology to map geomorphic riparian boundaries, 2) evaluation of the relative cost and utility of using topographic data of varying spatial resolutions to map riparian zone boundaries with this methodology, referred to as the Geomorphic Riparian Extent Model (GREM), and 3) evaluation of the relative cost/benefit of utilizing manually-interpreted (aerial photography) versus the combined used of GREM and computationally-classified (airborne or satellite remote sensing) data of various spatial resolutions, such as Landsat and EMERGE, to map riparian habitat. This report presents the findings of this study.

This study successfully developed a methodology to predict riparian geomorphic extents with the use of either a 10-m or 30-m digital elevation model (DEM). This methodology was used to predict riparian extent in 5 pilot watersheds in southern California using customized GREM models derived from fieldwork conducted in each watershed. In general, the GREM predicts riparian habitat particularly well in areas with high topographic relief or with narrow valley walls. It does not take into account the impacts of present-day hydrology on modern riparian habitat – and thus has a tendency to overpredict the extent of habitat in wider valleys or in areas that have been altered by anthropogenic modifications to the floodplain. This study also found that, while the 10-m DEM is preferable in terms of reducing modeling errors, a 30-m DEM could be used with acceptable levels of error to predict the geomorphic riparian extent. This distinction is important because for many areas of California a 10-m DEM is not currently available. A regional model was also developed and calibrated based on the physiographic characteristics of all five pilot watersheds. While the customized models for individual watersheds understandably have lower error rates in predicting riparian geomorphic extent, the regional model can be used to predict riparian extent in southern California watersheds without further necessity for fieldwork and model development, thus making the use of this methodology more cost-effective.

Comparison of GREM + Landsat mapped riparian habitat versus maps derived from manual interpretation of aerial photography provided a good mechanism for understanding tradeoffs between map accuracy, quality of information provided by the map, and cost. Notably, the regional GREM model, in combination with Landsat ETM-derived estimates of vegetative cover, represents a low-cost option for mapping riparian habitat (less than $500 per USGS 7.5 minute quad), approximately one-tenth of the cost of mapping riparian habitat using manual interpretation of aerial photography (approximately $5000 per USGS 7.5 minute quad). Thus, for an area such as that found within the WRP geographic scope (10,000 sq. miles or approximately 200 quads), the cost of mapping with GREM + Landsat would be roughly $100,000 versus $1 million using manually interpreted aerial photography. However, because of the definition of “riparian” employed by the GREM and how riparian extents are predicted, the delineated habitat represents “potential” or “predicted” habitat. As a result, the GREM + Landsat-derived vegetative cover is more useful as a screening tool to coarsely assess riparian habitat on a regional or statewide scale. Managers who require more detailed and accurate information about the riparian habitat, i.e. riparian habitat boundaries for regulatory use planning, local land use planning, or composition of riparian vegetation, and who have adequate funding will be better served by maps derived from field-based approaches and/or manual interpretation of aerial photography.

This study also examined the question of the appropriate resolution of imagery to use to determine vegetative cover in combination with the GREM. Use of Landsat ETM (30-m pixel size) versus a

higher resolution multi-spectral imagery such as EMERGE (1 m pixel) is preferred in combination with the GREM because the benefit of increased resolution in mapping vegetative cover from EMERGE is greatly outweighed by the increased cost (approximately 18 times that of Landsat). Thus to keep GREM mapping of riparian habitat a low-cost option, Landsat ETM is the imagery of choice.

INTRODUCTION

Riparian areas serve critical functions for the health of entire watersheds and represent perhaps the most important habitat for a majority of biodiversity in the arid western United States (Legleiter et al. 2002). Nationwide, the extent of riparian areas has declined by 60%-75%; however, in the western U.S., some riparian areas have declined by as much as 90% to 95% (USDOI 1994). The majority of remaining western riparian systems are generally in poor to fair condition in terms of performing typical habitat functions, many are vulnerable to degradation from adjacent development, and tens of thousands of stream miles are in need of restoration (Tiner 1984; World Resources Institute 1990; Dahl and Johnson 1991). Riparian areas provide many of the functions and values traditionally associated with wetlands (Cowardin et al. 1979, Tiner 1984) and in arid and semi-arid regions of the southwestern U.S., are especially vital because they often provide the only permanent sites of high soil moisture and mesic vegetation, thereby acting as habitat oases on which a multitude of native wildlife species are totally dependent for survival (Warner and Hendrix 1985, Faber and Holland 1988). Their linearity (along rivers) also allows them to serve as corridors providing important migratory or dispersal routes for migratory fauna between otherwise fragmented habitat patches. Because of their disproportionate importance compared to other landscapes, riparian areas have been the subject of research, conservation, restoration, and land use planning and management efforts (Muller 1997).

One of the initial steps in most riparian assessment or management programs is to determine the extent of riparian habitat in the study area. Basic inventories and maps are critical to all biological studies regarding riparian extent and vegetative composition (Evans et al. 2002), biodiversity indices, or habitat ranges for aquatic and terrestrial fauna (Strager et al. 1997). They may also be used to identify and prioritize areas in need of protection, conservation or restoration (NWI 1998, Evans et al. 2002). Other uses for riparian maps include the identification of areas suitable as buffers for intercepting and retaining agricultural runoff or other polluted or nutrient-rich surface water (Narumalani et al. 1997). Unfortunately, many regions lack current, comprehensive maps of riparian areas. For projects covering small areas, conventional field-based mapping or aerial photo-interpretation may be suitable. But for projects covering whole watersheds or regions, such an approach may be too expensive or time-consuming (DiPietro et al. 2002, Legleiter et al. 2002), and remote sensing (via either airborne or satellite platforms) may be more useful.

Mapping riparian areas from remote sensing data is typically based on identifying the extent of hydrophytic vegetation based on its spectral signature. Two general approaches have emerged for mapping riparian land cover and vegetation. The first is image classification, where every pixel in an image is assigned to a particular class based on spectral similarities across one or more spectral bands. Image classification of multispectral remote sensing data, especially satellite data, has generally been found to be more useful for mapping broad land cover categories rather than vegetation communities or species (Muller 1997). Multispectral remote sensing data do not generally provide accurate classified maps of riparian vegetation species or communities (Muller et al. 1993, Jamieson et al. 2001), unless multiple imagery dates are utilized (Townsend and Walsh 2001). This because the bandwidth in multispectral data is too broad to be sensitive to the more subtle changes in color that represent different communities or species. For this reason, land cover or land use derived from multispectral satellite data, vegetation is generally grouped into broad categories such as deciduous forest, evergreen forest, shrub land, and rangeland (Muller et al. 1993). Image classification of hyperspectral imagery can yield classification of individual plant species and communities (Leigleter et al. 2002, DiPietro et al. 2002), but is a more costly and time-consuming process.

The second general approach for mapping riparian land cover and vegetation with remote sensing data is the development of indices that can be correlated to a range of variability of some feature on the surface of Earth. The most common indices are vegetation indices such as the normalized difference vegetation index (NDVI). This index represents the range of greenness or vigor of vegetation, without attempting to categorize pixels into named vegetation classes. Various studies have shown correlations between remotely sensed vegetation indices and ground measured leaf area index, standing biomass, canopy cover, and other measures of vegetation (Tucker 1979, Nagler et al. 2001, Qi et al. 2000). However, no index has proven to be universally precise in identifying the extent of riparian habitat.

A major shortcoming of most remote sensing based riparian mapping is the failure to evaluate the lateral extent of the floodplain, the spatial extent of flood disturbance, and the variation of vegetation associated with flooding across the floodplain (Muller 1997). In the low gradient portions of watersheds in arid landscapes, riparian vegetation is often spectrally or visibly distinct from upland vegetation because of the greater vigor or biomass of riparian vegetation (Weber 2001). However, this is not always the case, especially in areas with rugged, mountainous landscapes such as the coastal watersheds of southern California. In these landscapes, upland vegetation on shaded slopes is at least as vigorous as, or spectrally similar to, the riparian vegetation; consequently, determining the width of the riparian zone using remote sensing may be particularly difficult (Inlander 2002, Goetz 2001, Russell 1997, Hewitt 1990).

In such cases, it is typical to delineate the width of the riparian zone by placing a distance buffer on the stream network using either a single-width or multiple-width buffering system. Single-width buffering scenarios use the same buffer width on all streams. Multiple-width buffers, or ‘smart’ buffers (Evans et al. 2002), use differing buffer widths depending on various attributes of the stream network, such as stream order, or other landscape characteristics. However, neither of these buffering systems may accurately capture the variability or complexity of the floodplain width (USFS 2005, Inlander 2002; Goetz 2001, Evans et al. 2002). Consequently, many riparian maps produced using remote sensing and stream buffers underestimate the actual extent of riparian habitat and fail to account for the dynamic nature of riparian ecosystems.

Some techniques utilize more advanced approaches for mapping the riparian zone boundary. Several approaches utilize a digital elevation model (DEM) and other ancillary datasets to identify a topographic break that is synonymous with the riparian zone boundary (Goetz 2001, WV GAP 2002). Inlander (2002) used this technique to develop a GIS-based model to map riparian areas in the upper Santa Ynez River watershed in Santa Barbara County, California – a rugged landscape where the valley is very flat relative to the upland hillslope. In flatter, more topographically homogenous landscapes, the edge of the valley is generally less dramatic or pronounced, and is more difficult to detect using a DEM. In such cases, delineation is often based on aerial photography interpretation (Evans 2002), digital image interpretation (Weber 2001), soils maps (Jones and Stokes Associates 1998), or other available ancillary data. Once the riparian zone boundary is delineated, most projects characterize riparian vegetation within that boundary using remote sensing or aerial photography data.

The goal of this study was to develop and test a three-step approach to riparian mapping that can be effectively implemented at a regional scale to cost-effectively map both the linear and lateral extents of riverine riparian areas from headwater streams to broad floodplain valleys. The methodology produces not only the stream network, but defines potential riparian zone geomorphic boundaries based on a series of DEM-derived topographic indices. Where necessary, the geomorphic boundary is edited to reflect anthropogenic alterations to the floodplain extent. Once the riparian boundaries are mapped, vegetation is characterized using remotely sensed vegetation indices to designate percent cover of riparian vegetation. The specific objectives of this study were to:

- Refine the methodology from Inlander (2002) for mapping riverine riparian zone geomorphic boundaries and canopy cover,
- Test the methodology in five pilot watersheds in southern California,

- Compare this methodology to other riparian mapping approaches, and
- Evaluate the relative costs and benefits of utilizing the various methodologies.

METHODS

Definitions of Terminology Used in Study

Because a primary objective of this project was to accurately delineate boundaries of the riparian zone, it was critical to establish a working definition of the term "riparian zone". Throughout scientific literature and applications, there is a "diverse and often confusing array" of definitions for riparian areas (Gregory et al. 1991). This diversity of definitions is due to the complexity and diversity of riparian areas as well as the variety of research and management contexts for which riparian areas are being defined (Goodwin et al. 1997, NRC 2002).

While many definitions for riparian are based on vegetative characteristics, others are based on geomorphic context. Riparian areas are commonly defined as the geomorphic features that are influenced by the adjacent aquatic system, especially in stream and river systems (NRC 2002). Floodplains are often considered synonymous with riparian areas (NRC 2002). The floodplain is the deposit of alluvium that covers a valley flat or valley bottom (Ferren 1996). The floodplain may include channels, the depositional areas, and terraces (Harris 1997). The floodplain interfaces with, and extends to, the valley walls (Bloom 1991). For example, Smith et al (2000) consider the riverine riparian zone to extend all the way to the valley edge, including less frequently flooded or abandoned floodplains and terraces.

This definition is logical because, although these outward features are not regularly inundated by superficial flows, the water table is generally shallow as compared to adjacent upland areas, thus influencing soil and vegetation characteristics (Bren 1993). For the purposes of this project, the riparian zone is considered synonymous with the floodplain or valley floor of fluvial systems. The edge of the riparian zone is synonymous with the valley edge. Although riparian habitat may occur along the edge of estuarine, lacustrine and depressional wetlands, this methodology only applies to mapping of riverine riparian habitat. Mapping based on this geomorphic definition will produce the maximum potential lateral extent of the riparian area and may represent the historic extent of river channel migration and its associated habitat.

Overview of Methods

For this project, methodology for mapping riparian areas consisted of two major steps as defined by Inlander (2002). The first step was to map the extent of the riparian zone using USGS DEMs. The second step was to characterize vegetation canopy cover within the mapped riparian zone using remote sensing imagery.

Mapping the geomorphic boundary or extent of the riparian zone consisted of several methodological steps: 1) DEM processing, 2) field data collection of valley transects for model calibration, 3) model development to predict the riparian zone extent based on field transect, 4) validation of the extent using additional field transects, and 5) editing for contemporary anthropogenic hydrologic alterations on the floodplain. This was done for each of five pilot watersheds in order to produce a customized model for each. It was also done for all pilot watersheds combined to produce a regional model. The intention was that this regional model could be applied to southern California coastal watersheds without further data collection to generate a customized model. In addition, models based on a 30-m DEM were compared to those of the 10-m DEM in the Ventura River watershed. This was done to test the effect of DEM spatial resolution on model accuracy, since 10-m DEM are currently not available in many areas of California.

Two remote sensing imagery products were used to characterize vegetation canopy cover within the modeled riparian zone. Landsat ETM (30-m spatial resolution) and EMERGE (1-m spatial resolution) imagery were used to generate vegetation indices. The vegetation index values we compared to field-measured canopy cover values. Linear regressions were used to scale vegetation index values and to predict canopy cover values at validation locations. The accuracies of the two imagery products were compared at validation sites to assess the cost-benefit of using high- versus low-resolution imagery. The most accurate DEM-based riparian extent model for the Ventura River watershed was used to clip the two remotely sensed canopy cover images. The clipped images served as the final riparian maps. The final riparian maps were compared to other riparian vegetation and floodplain datasets for additional validation of both riparian extent and vegetation characteristics. Each step of this process is described in detail below.

Study Area and Pilot Watersheds

The overall study area for this project included southern California coastal watersheds. Within this study area, five pilot watersheds were selected for development of the methodology. These include one watershed from each of the five coastal southern California counties: Carpinteria Creek (CARP), Ventura River (VENT), San Gabriel River (SANG), San Diego Creek (SAND), and Escondido Creek (ESCO). The five pilot watersheds, when considered as a single area, are referred to as the region (REGION). Figure 2.01 shows the locations of the five pilot watersheds.

Figure 2.01 Location of five pilot watersheds within southern California coastal zone.

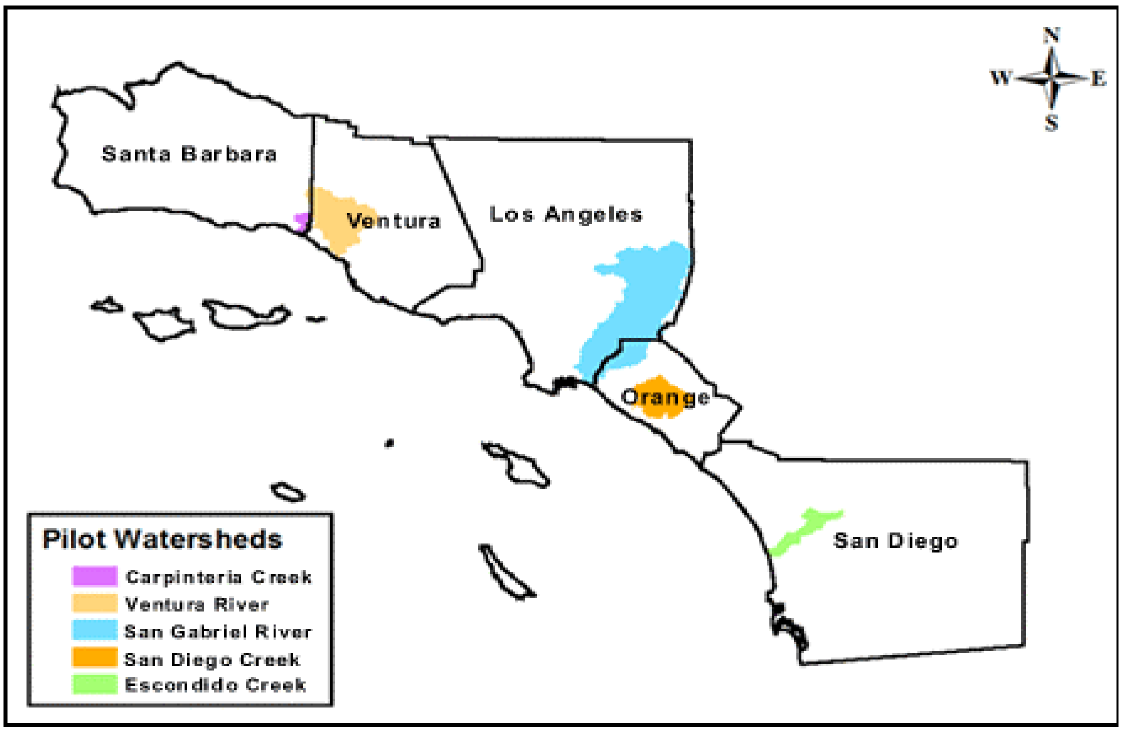

The pilot watersheds were selected to represent a range of physiographic settings as well as a gradient in urbanization, and thus vary greatly in terms of their size, topography, land cover, and ownership. Table 2.01 and Figure 2.02 describe the total area (km^2) and percent of each watershed in five slope classes respectively. At 39 km^2, CARP is the smallest of the pilot watersheds, making up only 1% of the five-watershed REGION. At 1747 km^2 SANG is the largest watershed, comprising 58% of the REGION. CARP and VENT have similar slope patterns, with approximately 70% of their areas in slopes greater than 20°. SAND and ESCO each have greater than 97% of their areas in slopes less than 20°. SANG has approximately 60% of its watershed in slopes less than 20° and approximately 40% slopes greater than 20°.

Table 2.01 Total area (km^2) of each pilot watershed or REGION in five slope classes. The size of each watershed is summarized at the bottom of the table.

Watershed Slope Class	CARP	VENT	SANG	SAND	ESCO	REGION
I (00 - 10)	5.2	78.0	848.6	327.5	120.6	1379.8
II (10 - 20)	5.1	97.6	198.3	66.7	96.0	463.6
III (20 - 30)	17.0	266.0	274.0	10.4	3.3	570.6
IV (30 - 40)	11.9	139.6	410.2	0.0	0.0	561.7
V (40 - 50)	0.0	3.4	16.4	0.0	0.0	19.8
Total	**39.1**	**584.5**	**1747.4**	**404.6**	**219.9**	**2995.5**

Figure 2.02 Percent of area of each watershed or REGION in each slope subclass. Range in

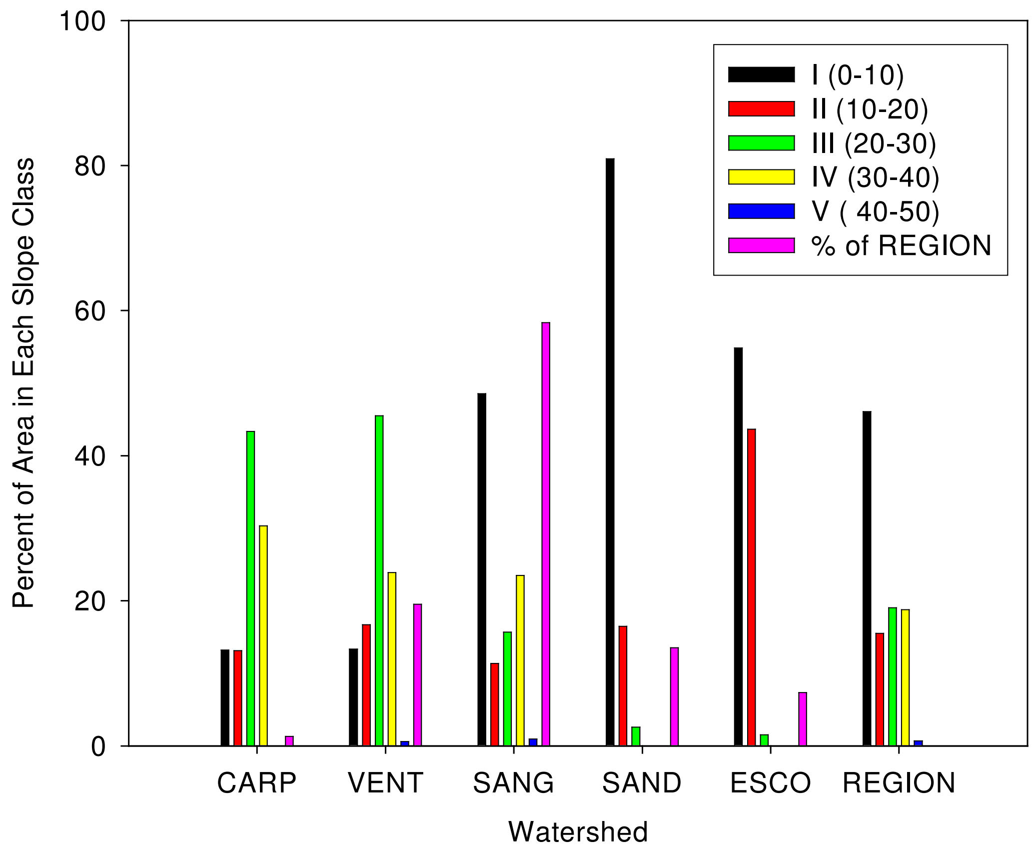

parenthesis represents degrees of slope.

Land cover was characterized using data from the NOAA Coastal Change Analysis Program (C-CAP), which utilized Landsat imagery from 2000 to map land use/ land cover into 38 classes. These classes were grouped into eight broad classes. Figure 2.03 summarizes the distribution of land cover types. Again, CARP and VENT exhibit similar patterns, with over 80% of their total areas in forest or scrub-shrub/chaparral. SAND is dominated by developed land cover, and SANG and ESCO also have significant developed areas. With regards to land ownership, CARP and VENT again exhibit a similar pattern, with approximately 50% public ownership. SANG has approximately 40% in public ownership, while SAND and ESCO have less than 10% each.

Figure 2.03. Percent of area of watershed or REGION in each land cover class

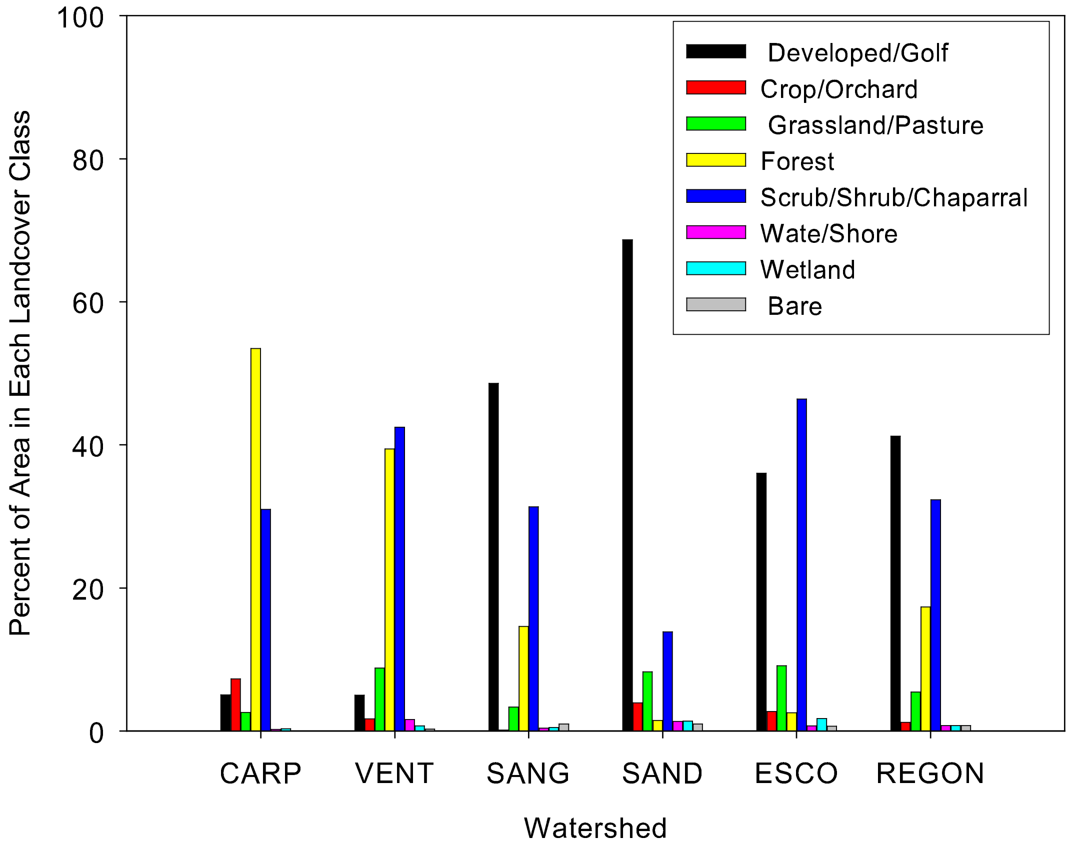

Digital Data Collection and Processing

Digital Elevation Models

The USGS 10-m DEM data served as the primary digital data source for modeling riparian zone extent in the five pilot watersheds. The 30-m DEM was also used to develop a model for VENT. Initially, DEMs were built from individual tiles and were smoothed with a single low-pass filter to reduce high-frequency noise and 'ripples' inherent in the data (Russell 1997).

Figure 2.04 gives an overview of the processing steps for the USGS DEMs. The filtered DEM was used to generate a stream network using standard Arc/Info command-line hydrologic modeling tools and ArcHydro. A flow accumulation threshold of 250 cells (2.50 ha) was used for the 10-m DEM, and a threshold of 28 (2.52 ha) cells was used for the 30-m DEM. Each DEM was reconditioned by "burning in" USGS 1:24,000 National Hydrography Dataset (NHD) streams. This corrected some erroneous

DEM-based stream delineations in relatively flat areas. Stream orders were assigned to the stream network according to the Strahler (1957) method. Nested subwatershed units (SWU) were generated for each stream order resulting in multi-scale sub-basins across the entirety of each watershed (Figure 2.05).

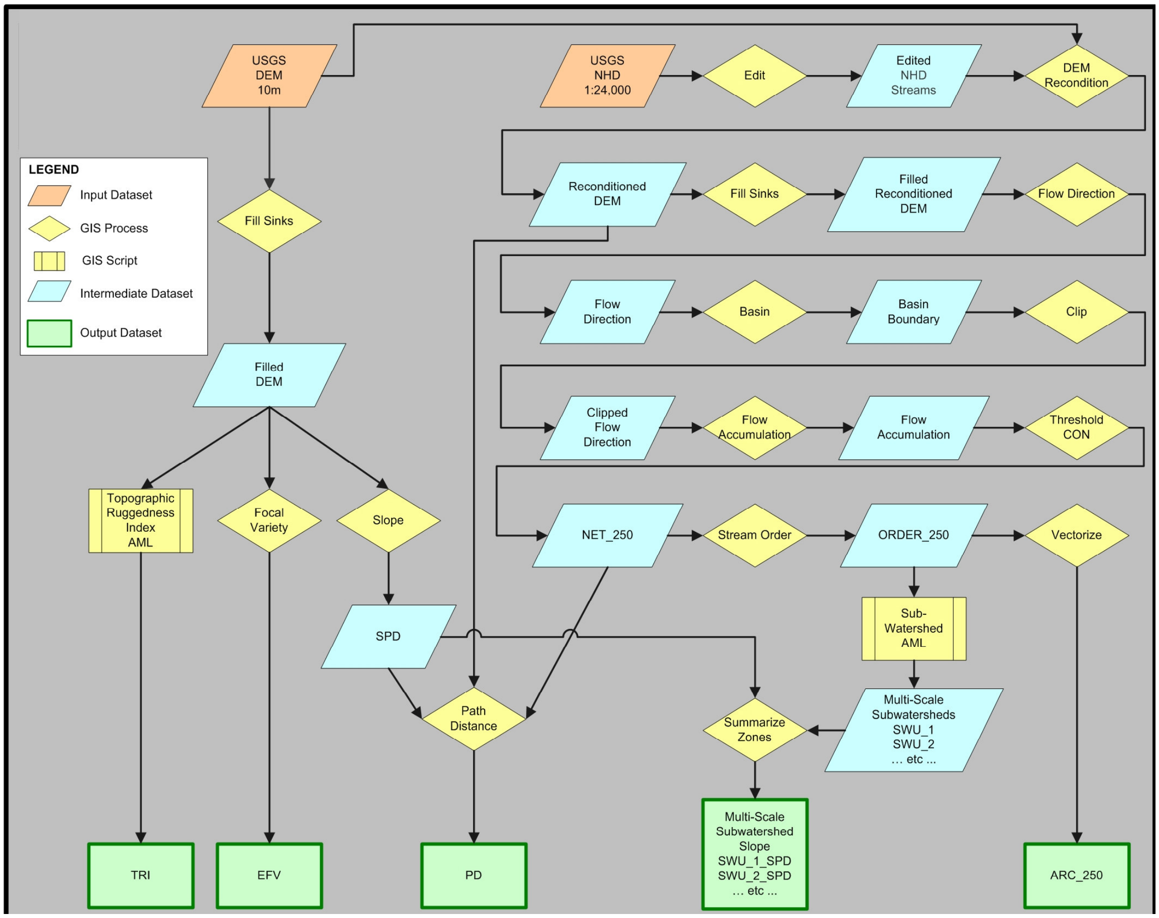

Figure 2.04 Diagram illustrating the processing steps for the USGS DEMs.

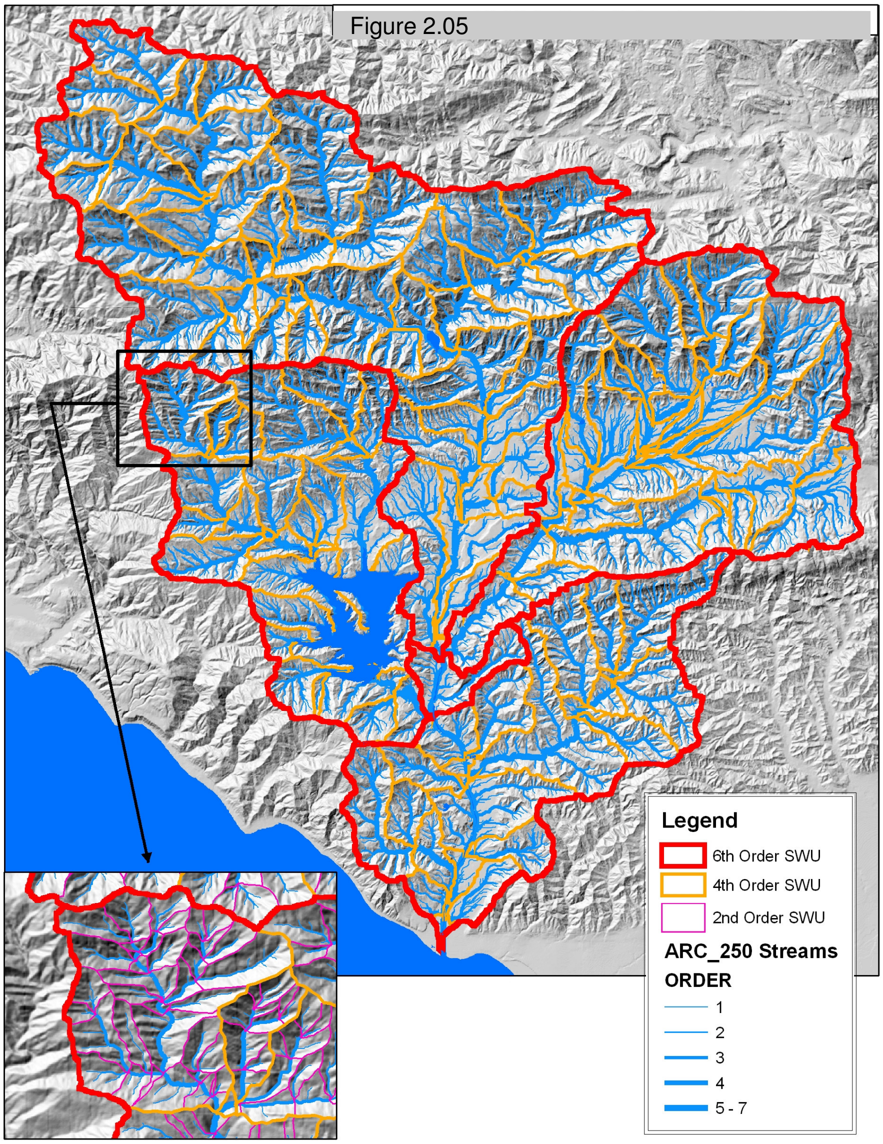

Figure 2.05 Map of the VENT watershed illustrating nested subwatershed units generated for each stream order.

Three DEM-derived geomorphic indices were produced in order to identify the topographic breaks between the valley floor and upland areas that serve as the lateral boundaries of the modeled riparian zone. The Elevation Focal Variety (EFV) index (ESRI 2005) measures the variety of integer elevation values for a cell and its eight neighbors. The Terrain Ruggedness index (TRI) (Riley et al. 1999) is a DEM derivative used to measure the amount of elevation difference between a cell and its eight surrounding neighbors. The TRI provides more information about a traditional slope measure because it assesses the vertical change taking place in the terrain model from cell to cell, as opposed to general steepness or gradient (NSTC 2001). The Path Distance (PD) index (WVGAP 2002) represents the topographic "cost" or difficulty of moving laterally or vertically away from the stream network. Sample results of these three indices are shown in Figures 2.06 a-c.

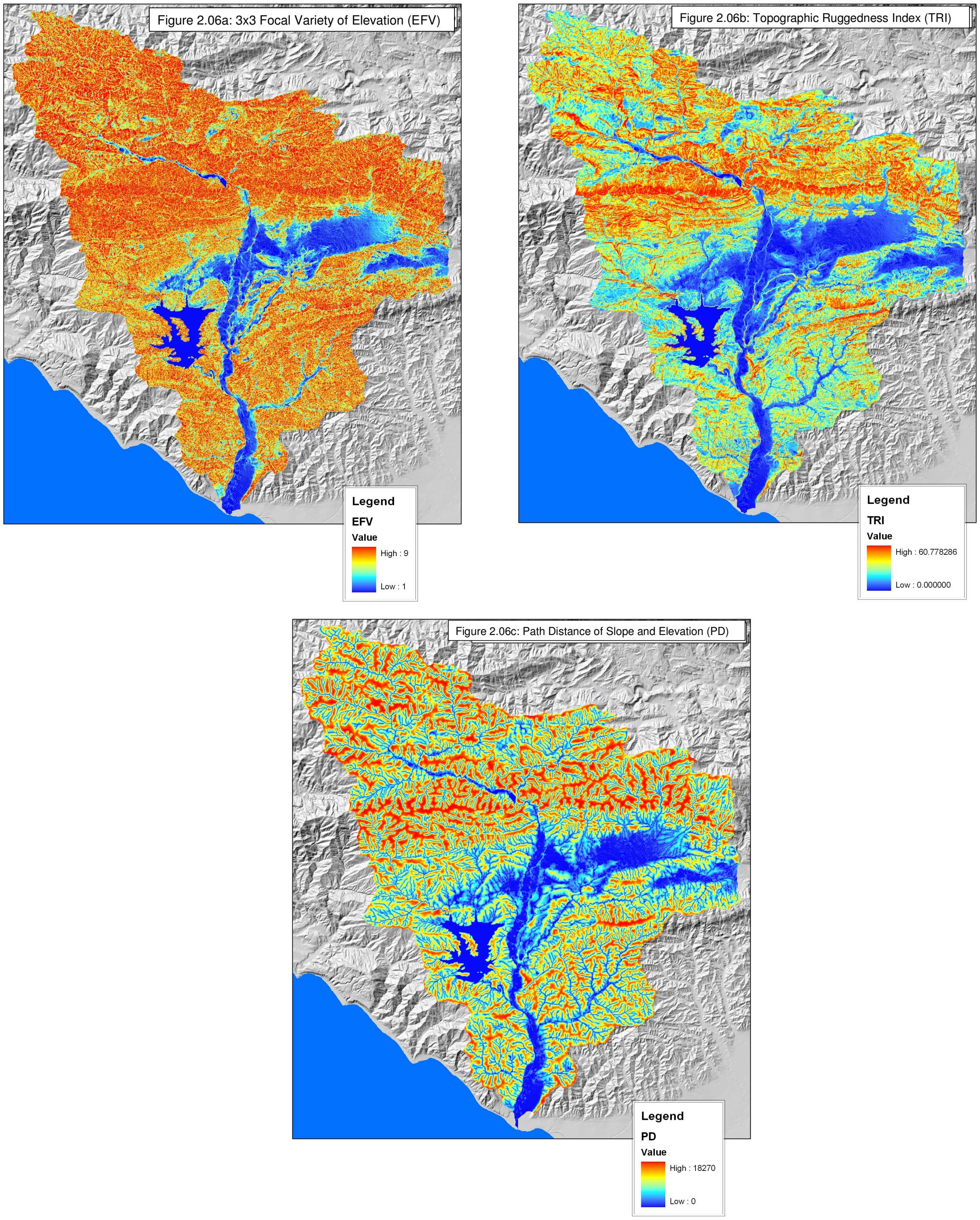

Figure 2.06(a-c).Graphical representation of EFV, TRI, and PD indices in the VENT watershed.

Each geomorphic index was further processed to generate various threshold grids for later modeling of the extent of the riparian zone (example shown on the left half of Figure 2.07). The values of the threshold grids are the means by which topographic breaks between the valley floor and upland areas are identified. Specifically, a threshold grid is a binary grid (cell values = 1 or 0) where cells of the original geomorphic index are less than or equal to (LE) a threshold value. For example, the binary threshold grid EFV_LE_05 had cell values of 1 where the original EFV cells had values of less than or equal to 5. All other cells in the EFV_LE05 grid have values of 0. Figure 2.08 shows threshold grids values on EFV of 3, 5 and 7. In any given threshold grid, cells with values of 1 were hypothesized to be valley floor, and cells with values of 0 were hypothesized to be upland. Threshold grid values ranged from 2 to 8 (in steps of 1) for EFV, from 2 to 20 (in steps of 2) for TRI, and from 100 to 600 (in steps of 20) for PD. A total of 42 threshold grids were generated for the three geomorphic indices in each pilot watershed. The accuracy of the threshold grids for each of the three geomorphic indices in predicting valley floor width and location was then evaluated.

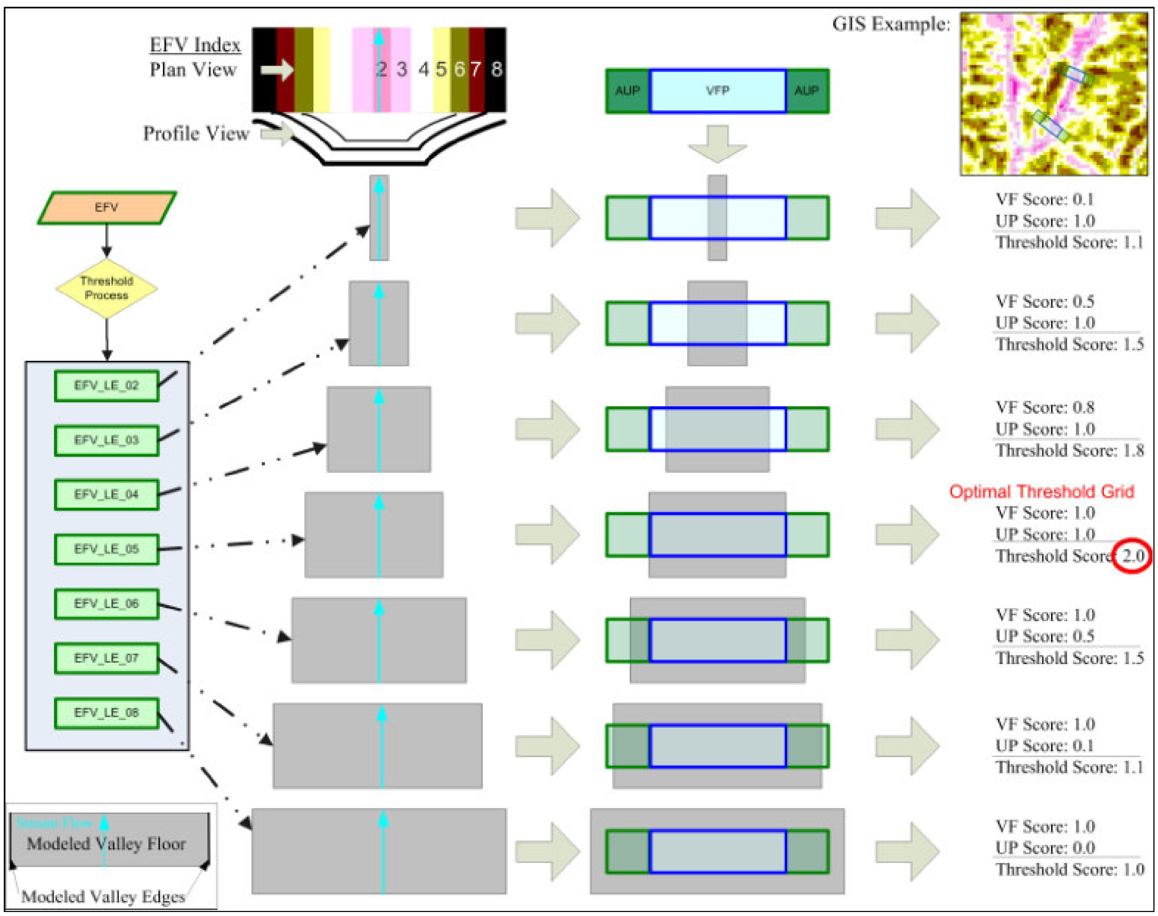

Figure 2.07 Process to establish optimal thresholds for each model.

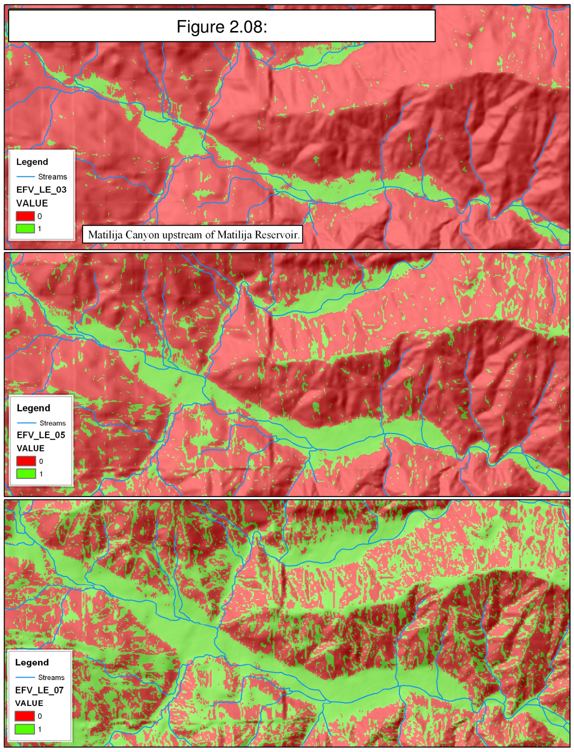

Figure 2.08. Threshold grids showing binary threshold values for EFV of 3,5, and 7 in each panel respectively.

Remote Sensing Imagery

Analyses of remote sensing data resolution with respect to riparian vegetative cover estimate accuracy were performed in the VENT pilot watershed. EMERGE multi-spectral digital airborne imagery was collected in August of 2003 in this watershed. Imagery was collected in three bands, which approximate Landsat ETM (ETM) bands 4, 3 and 2. The imagery was geometrically and radiometrically corrected by the EMERGE contractor. The cell size of the delivered imagery was 0.9 m. Horizontal errors varied from 1 to 5 meters depending upon terrain displacement within the landscape. A NDVI image was generated based on Eq. 2.1, which follows:

$$\mathbf{NDVI = ((Band4 - Band3) / (Band4 + Band\ 3))} \qquad \textbf{Eq. 2.1}$$

ETM data acquired on August 12, 2000, were obtained from USGS by NOAA Coastal Services Center for the C-CAP mapping of coastal California land use/land cover. The data provided were geometrically corrected to level 1G by USGS, and were found to have horizontal errors of up to 250 m. All ETM bands were clipped for VENT, and were geo-referenced in ESRI ArcGIS Desktop. The primary referencing layers were USGS NHD 1:24,000 scale streams and TIGER 2000 1:100,000 scale roads. A residual root mean squared (RMS) horizontal error of 18 m remained after geo-referencing, slightly greater than one-half of the 30-m pixel width. An NDVI image was generated based on Eq. 2.1, above.

The NDVI equation yields images with cell values with a maximum range of -1.0 to 1.0. Both the EMERGE and Landsat ETM NDVI images were rescaled to have values ranging -100 to 100 to make values more manageable in later analyses. Negative NDVI values generally represent non-vegetated surface such as barren land and water features (USGS 2006).

Field Data Collection and Processing

The purpose of field data collection was to document the lateral extent of the riparian zone and use these data to train/ calibrate, and subsequently validate the GREM model accuracy in predicting its location. Between twenty-eight and forty-three field sites were selected in each watershed to represent the range of floodplain conditions. Figure 2.09 describes the conceptual site selection process within each pilot watershed. Within each major accessible subwatershed, sites were visited within each stream order and across the range of valley width and intensity of flood control effort. Sites were selected without regard for known or predicted vegetation characteristics, consistent with Brothers (1985) and Bendix (1992). Legal access to sites was an overriding criterion for site selection.

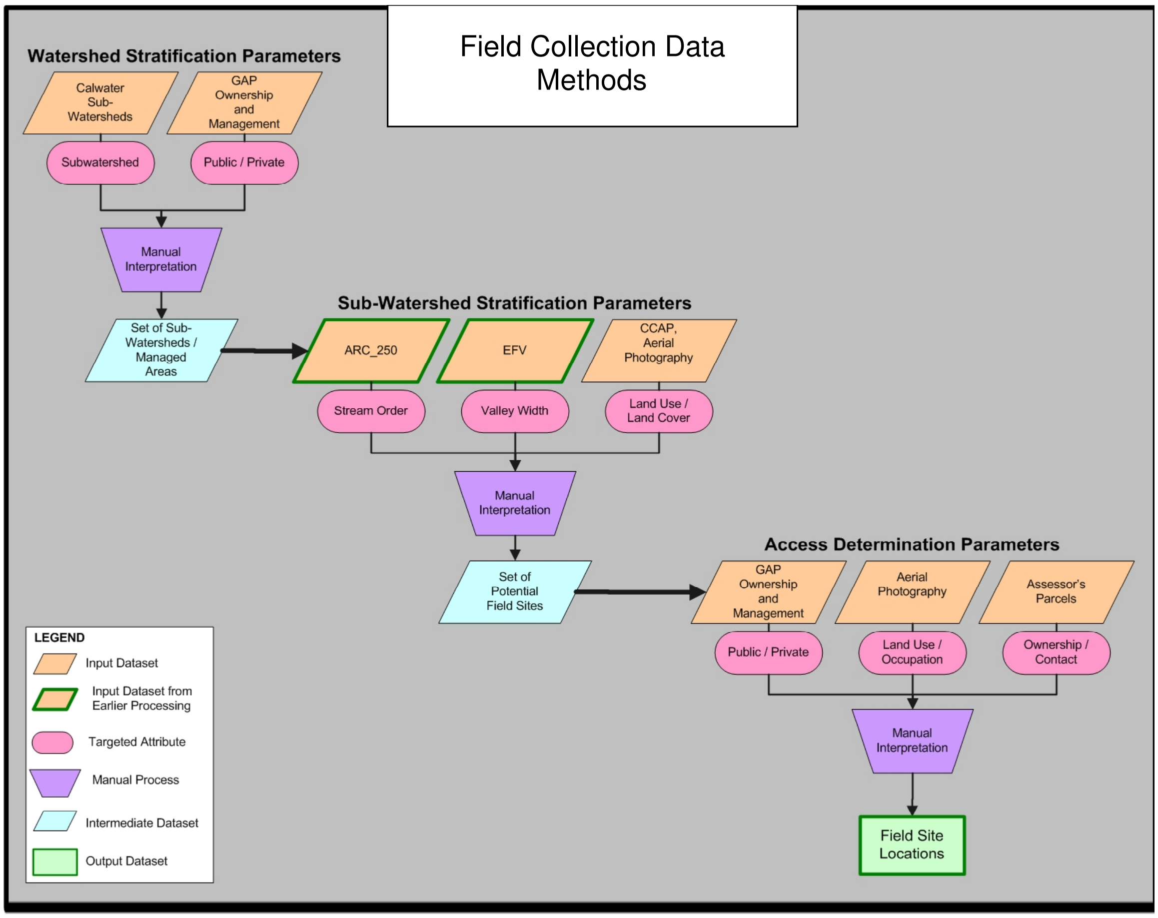

Figure 2.09 Diagram of field collection data methods within each watershed.

Once a site was located in the field, a transect was established perpendicular to stream flow extending from one valley edge to the other. The transect length was measured with either a tape measure or a laser range-finder. Valley edges were identified based on the slope break from hillslope to the valley floor. When the slope break was not obvious, it was interpreted from secondary indicators such as evidence of flooding or vegetation distribution. When present, human-made levees were mapped as the valley edge.

Each transect was subdivided based on prominent geomorphic features such as channels, banks, benches, and terraces (Figure 2.10). The edges (Geomorphic Break Point) and middle of each subdivision (Geomorphic Mid Point) were logged in a Garmin GPSMap 76S handheld 12-channel, WAAS-enabled GPS (Figure 2.11a). At each GPS point, percent vegetation canopy cover was measured using a concave spherical densiometer. The reported positional error of the GPS measurement was recorded for later use.

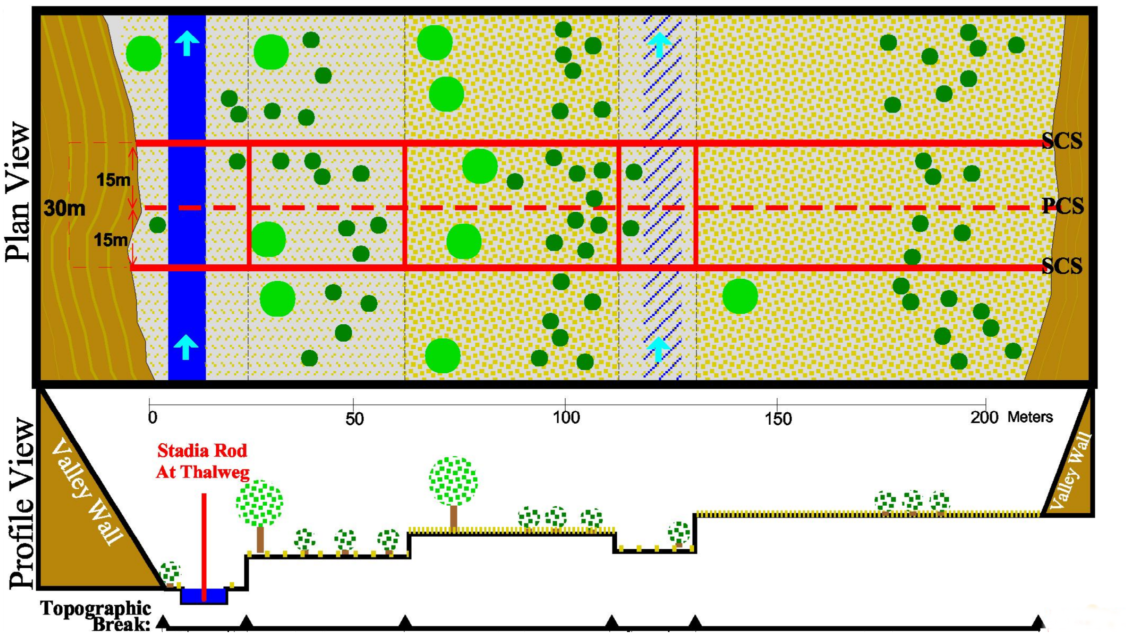

Figure 2.10 Schematic of locations of data collection with respect to channel geomorphology.

Data collected in the field were processed for GIS analysis. GPS waypoints were downloaded from the GPS unit to the office computer using Garmin Mapsource, Microsoft Excel, and ArcGIS Desktop. Transect GPS waypoints were used to generate transect line features, which connected only the two waypoints that represented the transect endpoints at the valley edges (Figure 2.11b). Canopy cover measurements were attributed to the GPS waypoints.

In each watershed, approximately one-half of the collected field sites were used to calibrate the riparian extent and canopy cover models, while the others were reserved for model validation. For each watershed, sites were assigned to a calibration pool and a validation pool using a stratified random process to ensure that both pools included sites in each subwatershed and sampled stream order. Within each watershed, several sites were excluded from analysis because their geomorphic characteristics could not be interpreted within the DEM riparian extent models.

Transects from the calibration pool were processed for later analysis of threshold values that were used to map the margin of the riparian zone, or valley edge (Figure 2.12a). Each transect line was buffered to generate a valley floor polygon. A 15-m “flat-full” buffer was used, which did not buffer beyond the end points of the original of the line (Figure 2.11c). A 45-m buffer was used for the 30-m DEM model (Figure 2.11d). To generate upland polygons, each transect was extended laterally 30 m from each end of the valley floor (as defined in the field) and then buffered with a 15-m (or 45-m) flat-full buffer. Each transect was assigned into one of three subwatershed slope classes (SSC) based on the average slope of the 2nd order SWUs it was located within (Figure 2.13). For example, the SSCs for VENT were SSC1 (0 to 20 degrees), SSC2 (20 to 30 degrees), and SSC3 (>= 30 degrees)

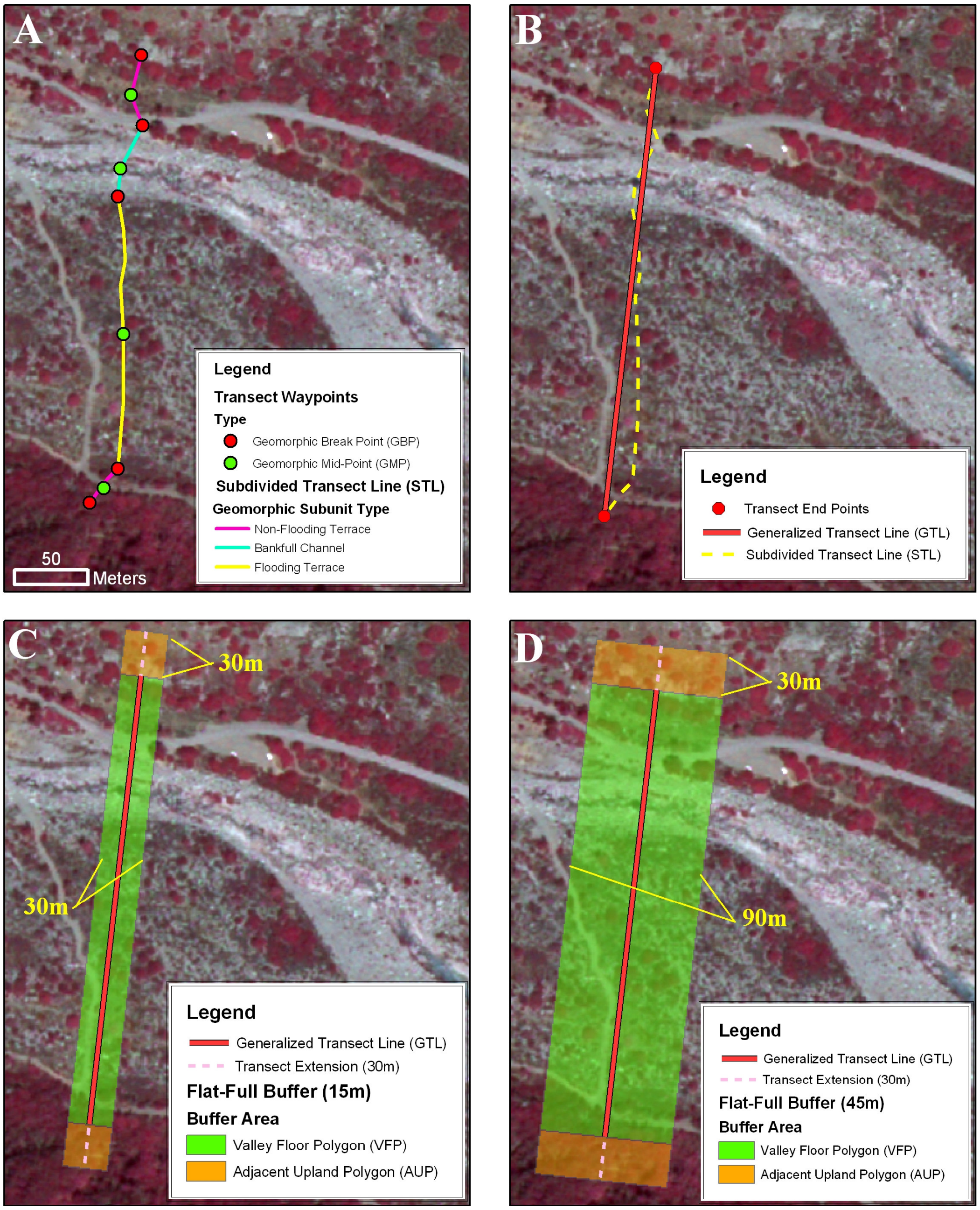

Figure 2.11(a-d). Illustration of steps to process transect data.

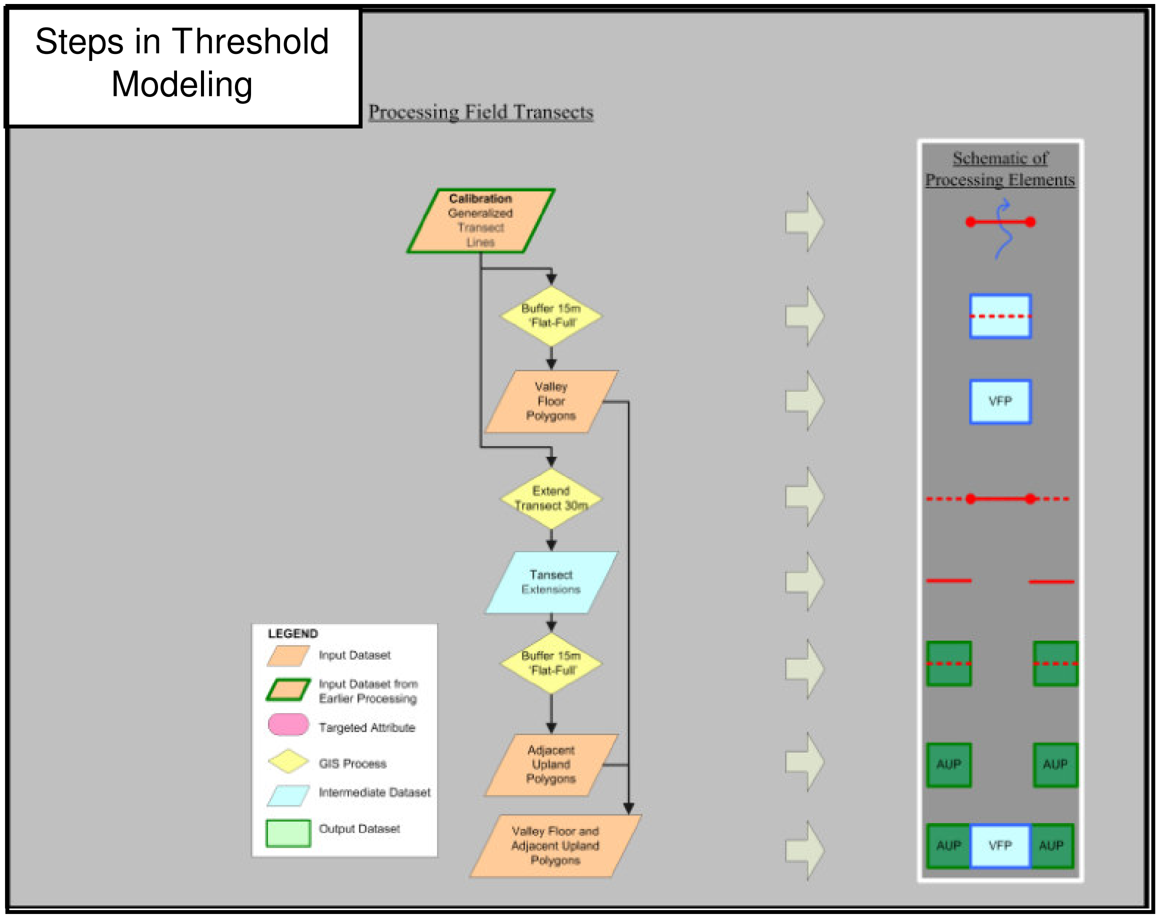

Figure 2.12 Steps to threshold modeling

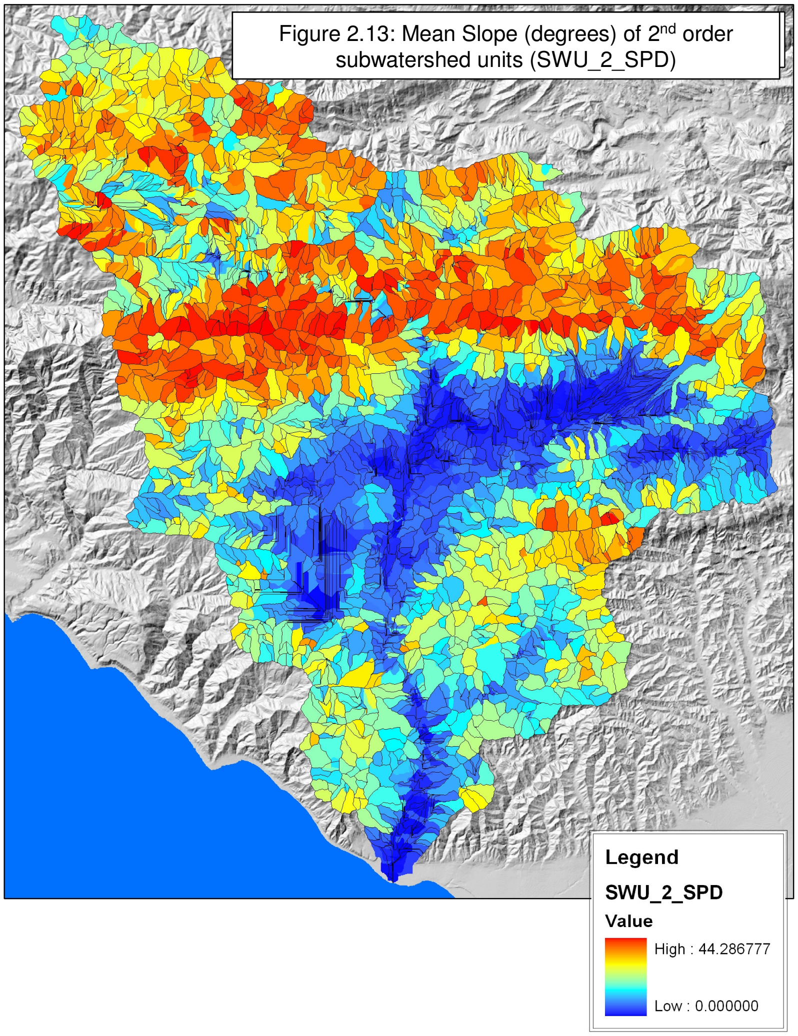

Figure 2.13 Slope classes of subwatershed units for the VENT watershed

Allocation of Field Sampling Effort and Stratification of Field Sites

Throughout the five pilot watersheds, data were collected at a total of 185 sites, with 43% of sites assigned for calibration, 36% for validation, and 21% excluded (Table 2.02). Excluded sites occurred on high stream orders, in low subwatershed slope classes, and with relatively broad field measured valley widths (Table 2.02). These sites generally occurred in the lower portions of the watersheds such as broad valleys with relatively subtle topography. Further, these areas are often urbanized or cultivated, and human-made levees often occur in these areas. These topographic and land-use characteristics cause the valley-floor models to perform inaccurately or fail completely, forcing sites in these areas to be excluded from analysis. Table 2.03 gives the average field-measured width of sites in each watershed. The VENT and ESCO sites were generally the widest, while the CARP were the narrowest.

Table 2.02. Allocation of field sampling effort by pilot watershed. Number of sites initially selected for calibration and validation of the models are given, as well the number of sites excluded from analysis modeling because anthropogenic impacts.

	SITE CATEGORY							
	Calibration		Validation		Excluded		TOTAL	
Watershed	**#**	**% of Total**	**#**	**% of Total**	**#**	**% of Total**	**#**	**% of Region**
CARP	12	43%	10	36%	6	21%	28	15%
VENT	19	45%	18	43%	5	12%	42	23%
SANG	19	44%	15	35%	9	21%	43	23%
SAND	10	29%	9	26%	15	44%	34	18%
ESCO	20	53%	15	39%	3	8%	38	21%
REGION	80	43%	67	36%	38	21%	185	100%

Table 2.03 Average field-measured width (in m) of sites by category. Calibration = CAL, validatoion = VAL, and excluded = EX.

	AVERAGE FIELD WIDTH BY CATEGORY			
WATERSHED	CAL	VAL	EX	ALL
CARP	57	49	84	60
VENT	114	100	205	117
SANG	73	72	123	83
SAND	41	34	289	90
ESCO	97	82	357	105
REGION	82	73	176	93

Regionally, 79% of sites were collected on 4th, 5th, and 6th order streams. Only 16% of sites were on 1st, 2nd and 3rd order streams, and only 5% of sites were collected on 7th and 8th order streams. The weighting of sites in the higher order streams was due to access issues. Table 2.04 shows that each five-degree slope class from 0-5 through 30-35 had 10%-17% of the total number of field sites, indicating that field sites were very evenly distributed across slope classes throughout the region.

Table 2.04 Number of field sites by slope class for each pilot watershed.

Watershed		CARP		VENT		SANG		SAND		ESCO		REGION	
		# of Sites	% of All	# of Sites	% of All	# of Sites	% of All	# of Sites	% of All	# of Sites	% of All	# of Sites	% of All
Slope Class in Degrees	00 - 05	6	21	5	12	2	5	12	35	3	8	28	15
	05 - 10			2	5	4	9	6	18	11	29	23	12
	10 - 15	5	18	2	5	3	7	6	18	14	37	30	16
	15 - 20			6	14	4	9	10	29	10	26	30	16
	20 - 25	5	18	11	26	8	19					24	13
	25 - 30	12	43	5	12	15	35					32	17
	30 - 35			11	26	7	16					18	10
	ALL	28	100	42	100	43	100	34	100	38	100	185	100

Modeling the Extent of the Riparian Zone

Threshold values for the DEM-derived geomorphic indices, EFV, TR, and PD, were used to develop a suite of geomorphic riparian extent models (GREMs). The models were initially calibrated using the calibration field sites. For the regional models, the calibration field sites of all five pilot watersheds were combined to run the threshold modeling process. In addition, hybrid models were developed by identifying the best performing model in each SSC, regardless of the topographic index source. In total, nine models were developed for each watershed and for the region. Once calibrated, the models were compared to data from the validation field sites to identify the most accurate model(s) for determining the extent of the riparian zone. The riparian extent modeling was completed for all pilot watersheds using the 10-m DEM, and was also completed for VENT using the 30-m DEM.

Threshold Scoring

Within each pilot watershed and regionally, two different threshold scoring scenarios were implemented to determine optimal threshold values for differentiating the valley floor from the adjacent upland. In the single threshold scenario (STS), an optimal threshold value was determined for all calibration sites of the watershed. In the multiple-threshold scenario (MTS), optimal threshold values were determined for calibration sites within each SSC (Figure 2.14). This allowed for the exploration of whether certain models performed better than others in varying landscape positions within the study area.

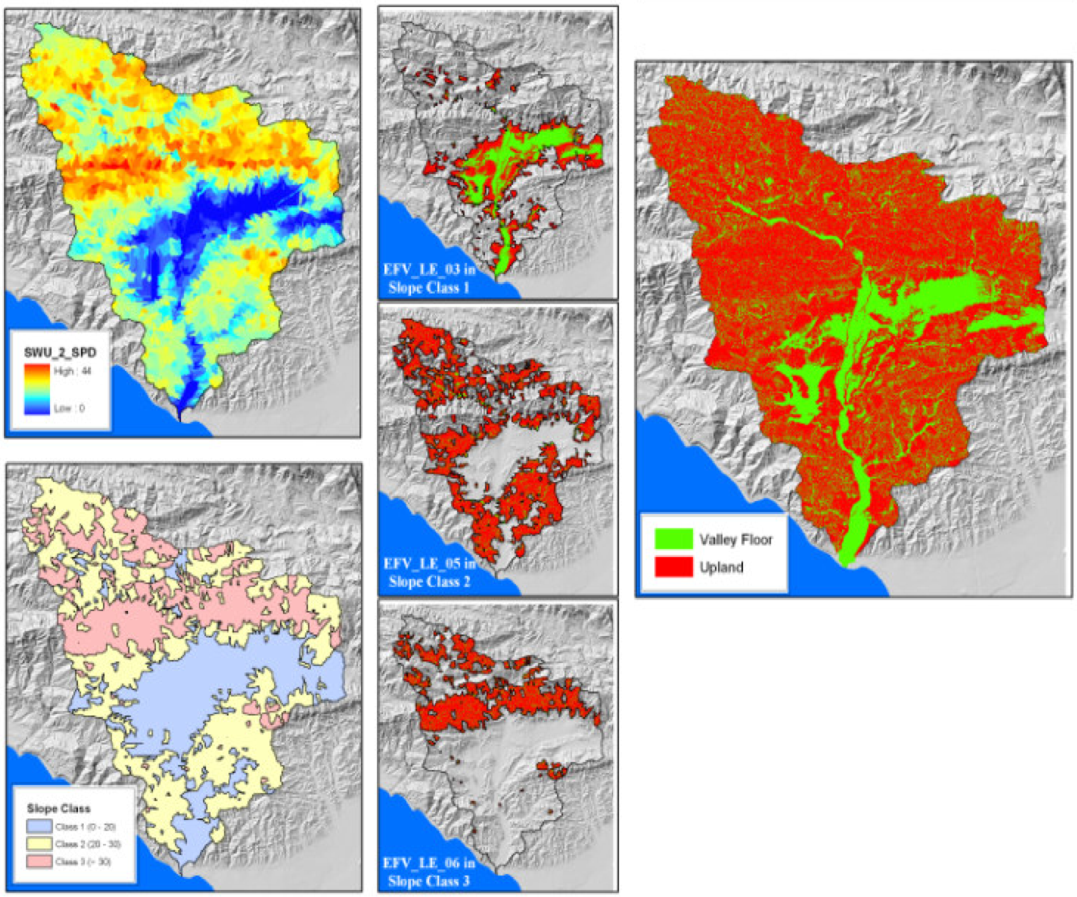

Figure 2.14 Processing steps for generating the EFV threshold grid for the multiple-threshold scenario

A threshold score was calculated for each threshold grid. The threshold score was comprised of a valley floor score and an upland score. The score was assessed by first aggregating the valley floor polygons and upland polygons of all calibration sites into a valley floor polygon aggregate and an upland polygon aggregate. These aggregates were then overlaid onto each threshold grid (right half of Figure 2.07). The valley floor score for a threshold grid was the proportion of the total area of the valley floor polygon aggregate that was hypothesized to be valley floor (cell values of 1) by the threshold grid. The upland score was the proportion of the total area of the upland polygon aggregate that was hypothesized to be upland (cell values of 0) by the threshold grid. The valley floor score and upland score were added to generate the threshold score which had a maximum possible value of 2.0, which would be reached if the threshold grid correctly identified all cells in the valley floor polygons as valley floor and all cells in the adjacent upland polygon as upland. In the STS, the threshold grid with the highest threshold score for all calibration sites was selected as the optimal valley floor model for each geomorphic index (EFV, TRI, and PD) yielding three STS riparian extent models. In the MTS, the optimal threshold grid for each geomorphic index was identified in each SSC, yielding three MTS riparian extent models.

Riparian Extent Model Generation

For the STS above, the optimal threshold grid from each geomorphic index was used to generate GREMs. An additional grid was generated by identifying areas as modeled riparian area only where the EFV, TR, and PD optimal threshold grids agreed. This grid, referred to as a confidence grid (CONF), was generated because a similar model proved to be the most accurate model in Inlander (2002).

The multiple-threshold grids were generated as described above, but based on the results of threshold scores in each SSC instead of in the data set as a whole. Figure 2.14 demonstrates the processing steps for generating the EFV threshold grid for the multiple-threshold scenario (EFV_MULTI). A similar process was used to generate the GREMs for the other two indices (TRI_MULTI and PD_MULTI).

A total of seven riparian extent models were tested for each individual watershed and then for all five watersheds combined (regional models). These included single and multiple-threshold results for each of the three geomorphic indices and CONF. Each grid was vectorized without generalizations. Polygons that did not intersect DEM-derived streams with a stream order greater that 1 were deleted. This eliminated many ridge top and other polygons in topographically high positions. The remaining polygons represented the areas hypothesized by each model to be riparian zone.

Assessing the Accuracy of Modeled Valley Floor Widths

For each of the seven valley floor models, model accuracy was assessed by comparing the modeled widths to field-measured widths. A modeled width was determined at each field transect by extending or truncating each endpoint of the transect line until it reached the modeled riparian edge (Figure 2.15). In some cases, the riparian extent models predicted no valley width in particular locations. Modeled widths at such locations were set to one-half of the width of the DEM cell (5 m in the 10-m DEM, 15 m on the 30-m DEM; Figure 2.16d. At confluences, the modeled width was determined by estimating the valley width at the transect location, while ignoring the confluence (Figure 2.15e).

Valley width model accuracies were assessed in terms of two error measurements: average absolute error (AAE) and root mean squared error (RMSE). These error values were calculated for each of the seven optimal valley floor models under the STS and MTS. Two hybrid valley floor models were identified and generated by selecting the most accurate model within each SSC regardless of the geomorphic index source. One hybrid utilized models with the lowest AAE in each SSC; the other utilized models with the lowest RMSE.

The seven original valley floor models, as well as the two hybrid models, were then compared to the field validation transects to determine the most accurate model for further use in the final riparian map. The overall accuracies for all validation sites were used to identify the best model. In all pilot watersheds, the valley floor model with the lowest validation AAE also had the lowest RMSE. Thus, the valley floor model with the lowest validation AAE and RMSE was selected for each pilot watershed and for the region as a whole.

Assessing the Accuracy of Modeled Valley Edge Locations

A second approach for assessing the accuracy of valley floor models was used only in the VENT. The distance from both edges of each field transect to the modeled valley edge were determined for all calibration and validation sites. Distances were measured regardless of whether the model overestimated or underestimated the transect width. These distances were averaged to assess the accuracy of the best performing models (HYB_RMSE (10-m) and TRI_MT (30-m)) for locating the valley edge. A total of 40

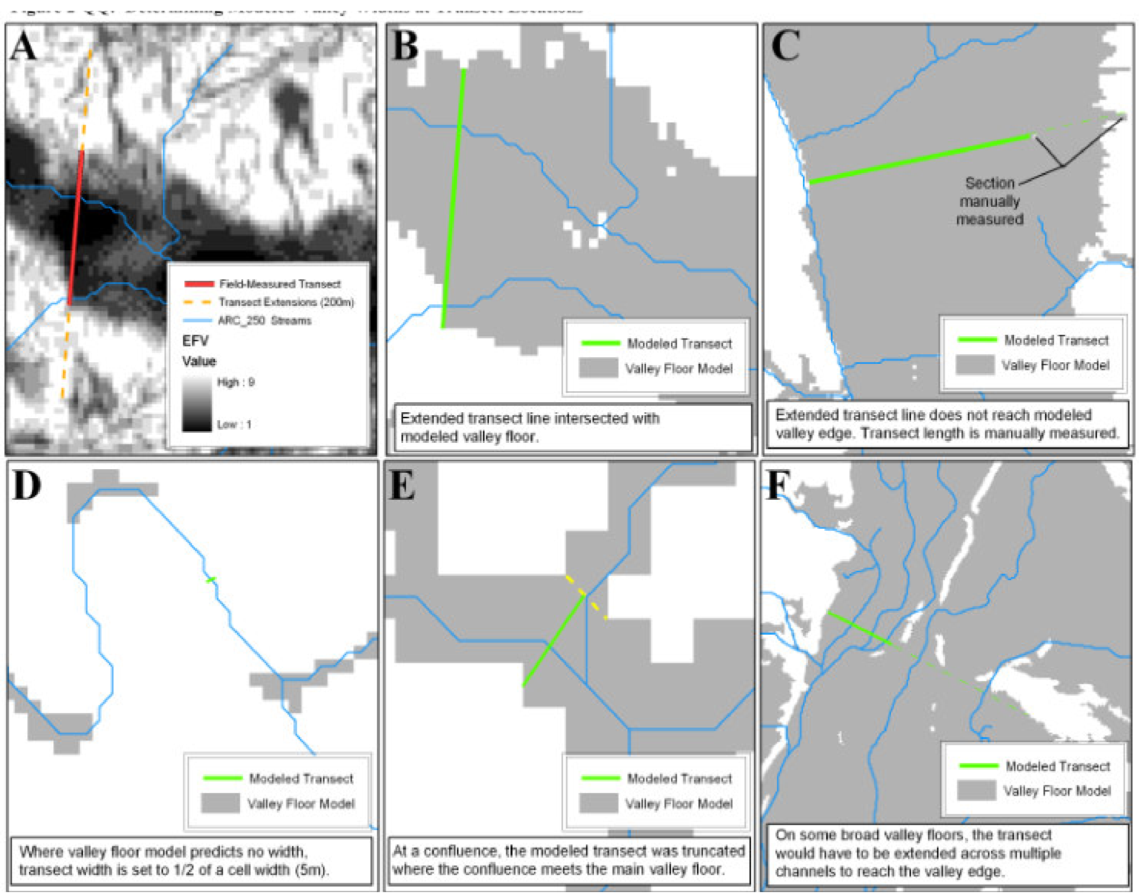

Figure 2.15. Procedure for determining modeled valley widths at transect location.

sites were included in the analysis. In cases where the TRI_MT model yielded a zero-width valley floor, a substitute was used. This substitute was a 7.5-m buffer on the 30-m DEM-based stream. This yielded a 15-m wide buffer, which was consistent with the half-cell width reset value in the width analyses.

Assessing the Accuracy of Modeled Valley Edge Locations

A second approach for assessing the accuracy of valley floor models was used only in the VENT. The distance from both edges of each field transect to the modeled valley edge were determined for all calibration and validation sites. Distances were measured regardless of whether the model overestimated or underestimated the transect width. These distances were averaged to assess the accuracy of the best performing models (HYB_RMSE (10-m) and TRI_MT (30-m)) for locating the valley edge. A total of 40 sites were included in the analysis. In cases where the TRI_MT model yielded a zero-width valley floor, a substitute was used. This substitute was a 7.5-m buffer on the 30-m DEM based stream. This yielded a 15-m wide buffer, which was consistent with the half-cell width reset value in the width analyses.

Editing the Selected Valley Floor Model

The valley floor model selected to have the best accuracies for VENT was edited to correct errors in the model in parts of the landscape where the model could not accurately map the valley floor. Such areas included urbanized, agriculturalized, leveed, and other modified areas in low-gradient portions of the pilot watersheds. In these areas, the DEM did not capture the features controlling the extent of the contemporary flood plain. Several GIS layers were used as ancillary information to edit the valley floor model. These included Federal Emergency Managemenet Agency (FEMA) floodways, National Resource Conservation Service (NRCS) Soil Survey Geographic (SSURGO) data, USGS NHD hydrography, NOAA C-CAP land cover, and current aerial photography. Areas that were historically part of the floodplain, but are contemporarily urbanized, agriculturalized, or have other significant human uses, were reviewed with the ancillary data. Generally, FEMA floodway data were used to edit the riparian extent model boundary in these areas. When FEMA polygons were suspect, aerial photography layers or field transect data were referenced. Once the mapped riparian areas were edited, many stream reaches, such as reaches that passed through urban or agricultural areas, had no riparian width. These areas were assigned a riparian width of 10 m by buffering the NHD streams and merging the buffer layer with the edited GREM layer.

Characterizing Vegetation Canopy Cover within the Modeled Riparian Extent

Vegetation canopy cover was characterized within the mapped (modeled and edited) riparian extent boundary for VENT using two remote sensing platforms. The EMERGE 1-m NDVI and ETM 30-m NDVI images were compared to field-measured canopy cover at calibration sites to identify correlations between field and spectral sensor measurements. Those correlations were used to develop linear regressions that predicted canopy cover across the mapped riparian extent. Canopy cover measurements at validation sites were used to identify and compare the accuracies of predicted canopy cover of both remote-sensing platforms.

Calibration

<u>EMERGE</u>

As described above, GPS waypoints from transects were attributed with their field-measured canopy cover values, which ranged fro 0 to 100%. A total of 70 GPS waypoints were collected at calibration sites. To compare field canopy cover measurements to NDVI values, image cell values were extracted for each GPS waypoint. But, the GPS positional accuracies of waypoints varied from three to twenty-two m, and averaged seven m. Consequently, the GPS waypoints were buffered by their reported positional error to generate a circular polygon around each GPS waypoint, or positional accuracy buffer polygon (PABP). The EMERGE NDVI cell values were averaged within each GPS accuracy polygon for all calibration waypoints to assign an NDVI value for comparison to field measurements.

Additional approaches for sampling NDVI values at field GPS waypoints were developed for comparison to the values assigned to the positional accuracy buffer polygons. Calibration GPS waypoints were also buffered by 3, 5, 7, 9, 11, 13, 15, 20, 25, and 30 m. These buffers are referred as # m buffer polygons (3MBP, 5MBP, 7MBP, etc.). Average NDVI values were attributed to each GPS waypoint separately for each #MBP scenario. Correlations were calculated between field-measured canopy values and averaged NDVI values for each buffer scenario.

The positional accuracy buffer polygon values were selected for development of regression formulas, though 7MBP had a higher correlation. The slope and intercept values of the linear regression equation were determined using Excel. The eq. 2.2 is given as follows:

$$\text{Predicted Canopy Cover \%} = ((\text{NDVI-PABP} * 1.2748) + 3.5813) \qquad \text{Eq. 2.2}$$

Landsat ETM

Because the positional RMSE for geo-referencing the ETM image was 18 m, and the average positional error of GPS waypoints was seven m, it was assumed that the specific ETM pixel within which the waypoints occurred could not be determined for field-to-image comparison. A 3x3-cell neighborhood averaging (3x3 focal mean, or FM3) filter was applied to the ETM NDVI image. NDVI values were then attributed to calibration GPS waypoints based on the NDVI FM3 image. A correlation was calculated between field-measured canopy values and NDVI FM3 values, and a linear regression equation was determined (Eq, 2.3):

Predicted Canopy Cover % = ((NDVI-FM3 * 1.8673) - 36.746) Eq. 2.3

Validation

Validation of predicted canopy cover values was carried out for predictions based on both EMERGE and ETM NDVI data. In each case, predicted canopy cover values at 81 validation GPS waypoints were calculated based on the calibration linear regression equations. These predicted canopy cover values were compared to actual canopy cover measurements at the validation GPS waypoints to assess the AAE and RMSE of predictions from both NDVI images.

Development of Final Riparian Maps

In order to produce the final maps, several additional processing steps were applied before combining the remote sensing canopy cover images with the final riparian extent model. The EMERGE and ETM predicted canopy cover images initially had some cell values less than 0% and greater than 100%. This was because the linear regression equations did not enforce a minimum or maximum predicted percent cover. To resolve this in the final images, values less than 0% were reset to 0% and values greater than 100% were reset to 100%.

These final predicted canopy cover images were clipped using the edited 10-m DEM riparian extent model. Because the ETM imagery has a cell width of 30 m, using it in this format would have degraded the final resolution of the ETM-based final map from 10-m to 30-m pixels. To avoid this, the ETM predicted canopy cover image was oversampled to 10-m cells before it was clipped with the final 10-m riparian extent model. Thus, the final GREM and ETM-derived riparian map had a cell size of 10 m, while the final GREM and EMERGE-derived maps had a cell size of 1 m; the original cell size of the EMERGE data.

Comparison of the GREM and GREM-Derived Riparian Map to Other Geomorphic and Vegetation Datasets

Both the unedited and edited GREM, as well as the GREM and ETM-derived maps, were overlaid with other datasets to compare extent, geomorphic, vegetative, and land use characteristics in VENT and to help assess accuracy of the model.

SSURGO Geomorphic Type

The unedited final 10-m GREM for VENT was compared to the NRCS Soil Survey Geographic (SSURGO) soils layer to demonstrate the types of landscapes mapped by the GREM. The “geomorphic description” attribute was used for this comparison. Geomorphic types were separated into groups that were valley or upland features. The ability of the unedited GREM to accurately capture the valley features was assessed. The SSURGO data was only available for approximately 45% of the VENT watershed because NRCS did not map soils within the Los Padres National Forest boundary. .

National Wetlands Inventory

The edited 10-m GREM and EMERGE GRECM for VENT was compared to the National Wetlands Inventory (NWI) riparian and wetlands GIS layer (NWI map) that was produced for SCCWRP by the US Fish and Wildlife Service (USFWS). This dataset was chosen as one representative of maps produced by manual interpretation of aerial photography. It uses a definition of riparian habitat that is based on vegetation. The NWI map was based on aerial photography interpretation flown in 2000. Riparian areas were classified based on modifications to Cowardin et al. (1979). This classification involved mapping riparian habitats that may be considered “wetland” as well that found in upland transitional zones. The NWI map was compared to the GREM by assessing AAE, RMSE and TAE of valley width for validation transects. Errors associated with the mapped riparian edge compared to the modeled valley edge in the GREM were also identified.

The NWI map was also compared to the final 10-m GREM and GRECM models in terms of extent, SSURGO geomorphic type, slope, C-CAP land cover, and NDVI values. These comparisons were made for the entire mapped areas as a whole, as well as by stream order. A stream order was assigned to each cell within the final GREM using a Euclidean allocation tool in ArcInfo Workstation. For each cell, the tool identified the closest stream arc and then assigned that stream order. Only streams with an order greater than one were used for the analysis.

The average value of ETM NDVI predicted canopy cover image was assessed for each wetland/riparian vegetation type in the NWI map to see if these descriptive types had quantitative differences and trends.

Multiple-Width Buffer Scenario

A multiple-width buffer scenario was proposed for the Ventura River watershed by Ferren et al (1995), and was based originally on Brinson (1993), to estimate the width of wetlands associated with the riparian corridor. An average width was calculated per stream order based of extensive field measurements. Ferren et al. (1995) found that first order streams had an average wetland width of 3 to 5 m. Second and third order streams had widths averaging 15 to 25 m. Fourth order streams had widths varying from 25 to 100 m. The fifth order reaches averaged 300 m wide, except for braided reaches, where the average width was 600 m. A buffer scenario based on these widths values was developed for the streams in the study area. Two scenarios were developed: one using the NHD stream network and one using the stream network derived from the 10-m DEM. These scenarios are referred to as the Ferren NHD and Ferren DEM datasets. The buffer widths for streams in the upper watershed were 4, 15, 25, 62.5, 100 and 300 m for 1st, 2nd, 3rd, 4th, 5th and 6th order streams, respectively.

Once the buffer was generated, it was compared to the final GREM in terms of total extent, AAE, and RMSE of valley width based on validation sites; errors associated with the mapped riparian edge compared to the modeled valley edge in the GREM.

RESULTS

Analysis of the geomorphic boundary and vegetative cover data addressed the following questions:

- How accurate are the GREM models at predicting the extent of the riparian zone?
- How does the 10-m DEM compare to the 30-m DEM in terms of accuracy?
- What is the accuracy and associated costs of using high-resolution (EMERGE) versus low resolution (Landsat ETM) imagery to map riparian vegetative cover?
- How well do the selected GREM models compare to methods employing manual interpretation of aerial photography (such as NWI) for mapping riparian areas?
- What are the associated costs with each?

Model Accuracy in Predicting Extent of Riparian Geomorphic Boundary

Optimizing Thresholds on Geomorphic Indices

Results for the regional threshold analysis for both the STS and MTS show that a single optimal value exist for each model, illustrated by the fact that each curve shown in Figure 3.01 has a single peak. The plots also show that threshold scores vary across slope classes. In general, the models have higher threshold scores in higher slope classes. Thus, the valley floor is generally more discernable from the adjacent upland in steeper landscapes. Results were similar for individual pilot watersheds.

In most watersheds, errors in modeling valley width were generally correlated to the actual valley width. This was the case in CARP, VENT, SANG, and ESCO, where the RSME was positively correlated to field-measured valley width (0.95 R^2). The trend did not hold true in SAND, where RMSE was greater than twice the average field-measured width.

Although each model had a single optimal value, none of the geomorphic indices resulted in a universal best-fit model. Optimal indices and thresholds varied by watershed and by slope subclass (Table 3.01).

For the single-threshold scenario analysis (STS), the highest scoring valley floor model was TRI for all watersheds using a 10-m DEM, with the exception of the SAND watershed. The best scores for CARP, VENT, SANG, ESCO, and REGION for TRI had threshold values of 6, 4, 6, 6 and 6, respectively. The highest score in SAND was from the EFV_LE_03 model. The highest score for VENT 30-m was from PD_LE_200.

For the multiple threshold scenario analysis (MTS), the highest scoring valley floor model was generally the PD, except for the Escondido watershed and the regional model, where TRI produced the best fit. In SANG, Slope Classes 1 and 3, the highest scoring threshold were from the PD model, but TRI model scored highest in Slope Class 2. For REGION, TRI received the highest threshold score in Slope Classes 1 and 2, while PD had the highest threshold score in Slope Class 3.

Six valley floor models were determined for each watershed or regional model. These six models were used for further analysis, along with the CONF model. These models are identified in Table 3.01 by the threshold values for all sites (STS) and for each Slope Class (MTS).

Figure 3.01 Threshold values and scores for REGION model in the VENT watershed.

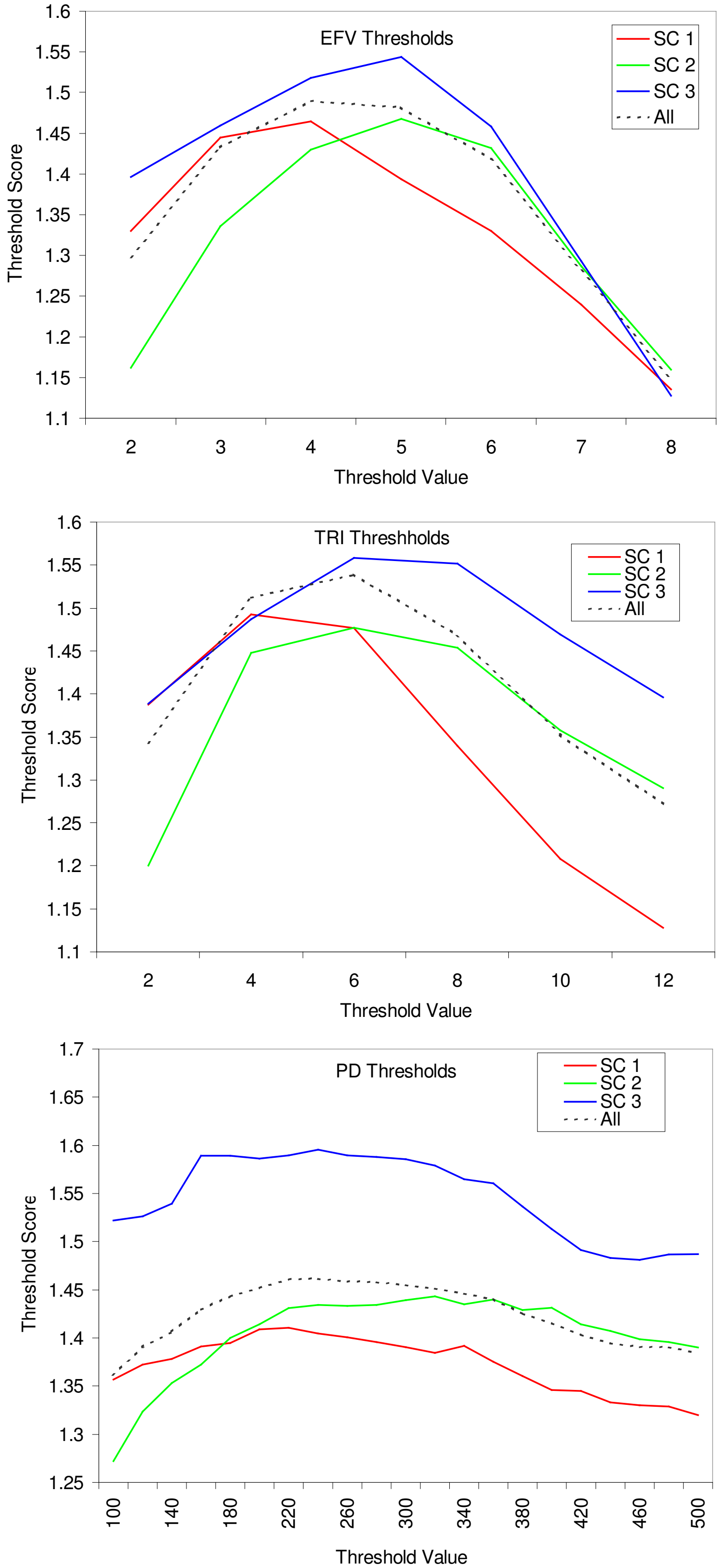

Table. 3.01 Threshold scores for geomorphic valley floor models. Bolded scores represent the highest threshold values.

		MODEL					
		EFV		TRI		PD	
CARP		Score	Threshold	Score	Threshold	Score	Threshold
	0 to 15	1.446	4	1.554	4	1.625	540
MTS	15 to 25	1.488	6	1.354	12	1.560	180
	> 25	1.360	6	1.368	8	1.587	200
STS	All Sites	1.586	5	1.590	6	1.504	500
VENT 10-m		Score	Threshold	Score	Threshold	Score	Threshold
	0 to 20	1.635	3	1.585	2	1.682	120
MTS	20 to 30	1.530	5	1.549	6	1.562	320
	> 30	1.401	6	1.346	10	1.407	260
STS	All Sites	1.581	3	1.5934	4	1.5927	160
VENT 30-m		Score	Threshold	Score	Threshold	Score	Threshold
	0 to 20	1.710	6	1.676	8	1.778	200
MTS	20 to 30	1.253	6	1.517	14	1.451	280
	> 30	1.457	7	1.331	10	1.399	400
STS	All Sites	1.530	6	1.5392	8	1.5681	200
SANG		Score	Threshold	Score	Threshold	Score	Threshold
	0 to 20	1.188	4	1.268	6	1.319	360
MTS	20 to 30	1.564	4	1.580	4	1.573	160
	> 30	1.326	6	1.487	10	1.618	480
STS	All Sites	1.474	4	1.497	6	1.489	280
SAND		Score	Threshold	Score	Threshold	Score	Threshold
	0 to 15	1.428	3	1.394	4	1.481	200
MTS	15 to 25	1.429	5	1.262	4	1.434	140
STS	All Sites	1.476	3	1.454	4	1.464	160
ESCO		Score	Threshold	Score	Threshold	Score	Threshold
	0 to 10	1.520	4	1.667	6	1.596	540
MTS	10 to 15	1.358	7	1.440	6	1.243	140
	15 to 20	1.493	6	1.539	8	1.439	240
STS	All Sites	1.447	6	1.596	6	1.420	340
REGION		Score	Threshold	Score	Threshold	Score	Threshold
	0 to 15	1.465	4	1.493	4	1.411	220
MTS	15 to 25	1.467	5	1.477	6	1.443	320
	> 25	1.544	5	1.558	6	1.595	240
STS	All Sites	1.489	4	1.539	6	1.462	240

Assessing Model Accuracy in Predicting Width of Valley Floor

Model Calibration

In model calibration, the best-performing models for each single threshold were selected for validation. In addition, the best-forming models during the calibration exercise in each SSC were the sources for the hybrid models (Tables 3.02 – 3.03). For example, the Hybrid based on minimizing AAE (HYB-AAE) for VENT 10-m included TRI_04 in Slope Class 1, EFV_05 in Slope Class 2 (the EFV threshold value for Slope Class 2 in the EFV_MT model, see Table 3.04), and PD_160 in Slope Class 3. A single HYB model was yielded from the analysis of calibration sites for CARP because the model with the smallest AAE in each Slope Class was the same model as with the RMSE. Effectively, the HYB-AAE and the HYB-RMSE were the same model. No Hybrid models were developed for ESCO because the components of TRI_MULTI performed best in each SSC, meaning that the HYB-AAE and HYB-RMSE were the same as the TRI_MULTI.

Table 3.02 Average absolute errors (AAE) for the geomorphic models during calibration for CARP, VENT 10-m , VENT 30-m, SANG, ESCO and REGION. The best performing models for each Subwatershed Slope Class are highlighted with bold text. The best performing models overall are also highlighted with gray fill. AFW = Average field width. The width analysis was not performed for SAND, though the field sites in SAND were included in the analysis for REGION.

	SSC	AFW							
CARP 10m	SSC	AFW	EFV_05	TRI_06	PD_500	EFV_MULTI	TRI_MULTI	PD_MULTI	CONF3
	Class 1	172	22.3	29.7	37.7	72.0	**16.0**	35.3	32.3
	Class 2	12	10.3	5.7	18.3	47.3	18.3	**1.3**	5.7
	Class 3	21	12.5	10.0	18.8	12.2	15.2	**9.8**	10.0
	ALL	57	14.4	**13.8**	23.4	35.9	16.2	14.1	14.5
VENT 10m	SSC	AFW	EFV_03	TRI_04	PD_160	EFV_MULTI	TRI_MULTI	PD_MULTI	CONF3
	Class 1	232	52.0	**17.4**	62.1	52.0	78.1	71.7	63.2
	Class 2	101	61.1	39.1	34.2	**25.3**	28.3	28.0	64.5
	Class 3	18	16.9	17.5	**6.1**	22.6	49.1	17.8	15.9
	ALL	114	47.1	**27.7**	34.2	31.6	46.9	36.8	51.4
VENT 30m	SSC	AFW	EFV_06	TRI_08	PD_200	EFV_MULTI	TRI_MULTI	PD_MULTI	CONF3
	Class 1	245	45.9	75.9	**25.9**	45.9	75.6	**25.9**	67.1
	Class 2	96	35.9	66.2	46.7	35.9	57.6	**34.8**	64.0
	Class 3	63	29.2	35.3	46.7	30.4	**22.0**	61.7	35.3
	ALL	114	**35.2**	54.1	42.3	35.7	44.8	44.2	52.6
SANG 10m	SSC	AFW	EFV_04	TRI_06	PD_280	EFV_MULTI	TRI_MULTI	PD_MULTI	CONF3
	Class 1	122	48.6	**7.7**	60.3	48.6	**7.7**	57.0	61.6
	Class 2	78	12.4	11.6	13.3	12.2	14.3	**10.5**	13.7
	Class 3	22	14.0	11.5	14.5	22.0	**9.3**	19.3	11.5
	ALL	73	18.5	**11.0**	21.0	20.1	12.2	19.7	20.8
SAND 10m	SSC	AFW	EFV_04	TRI_06	PD_240	EFV_MULTI	TRI_MULTI	PD_MULTI	CONF3
	Class 1	53	30.5	52.8	31.8	31.8	26.8	**19.3**	
	Class 2	23	14.5	93.3	35.3	**6.8**	55.8	49.0	
	Class 3	na							
	ALL	41	22.5	73.0	33.2	**20.7**	41.3	31.2	
ESCO 10m	SSC	AFW	EFV_06	TRI_06	PD_340	EFV_MULTI	TRI_MULTI	PD_MULTI	CONF3
	Class 1	160	42.6	**24.6**	48.3	69.2	24.7	42.4	49.0
	Class 2	59	31.9	**21.9**	40.3	80.2	21.9	30.4	26.1
	Class 3	45	34.7	18.4	17.2	34.7	**12.3**	21.7	18.4
	ALL	84	35.5	21.9	37.4	67.0	**20.5**	31.8	30.8
REGI 10m	SSC	AFW	EFV_04	TRI_06	PD_240	EFV_MULTI	TRI_MULTI	PD_MULTI	CONF3
	Class 1	118	40.3	**28.9**	42.4	40.1	33.7	39.8	
	Class 2	79	28.9	28.7	32.9	24.7	**24.6**	30.5	
	Class 3	42	11.7	11.2	10.5	12.2	11.2	**10.1**	
	ALL	82	27.7	**23.4**	29.8	26.3	23.7	27.9	

Table 3.03 Root square mean errors (RSME) for the geomorphic models during calibration. The best performing models for each Subwatershed Slope Class are highlighted with bold text. The best performing models overall are also highlighted with gray fill. AFW = average field width.

	SSC	AFW	EFV_05	TRI_06	PD_500	EFV_MULTI	TRI_MULTI	PD_MULTI	CONF3
CARP 10m	Class 1	172	29.4	41.7	48.5	100.1	**23.1**	46.9	39.8
	Class 2	12	15.8	10.7	25.1	76.4	25.1	**2.8**	10.7
	Class 3	21	15.6	12.7	21.5	18.1	28.1	**12.7**	12.7
	ALL	57	**17.7**	20.3	27.4	55.1	23.9	21.8	19.5
	SSC	AFW	EFV_03	TRI_04	PD_160	EFV_MULTI	TRI_MULTI	PD_MULTI	CONF3
VENT 10m	Class 1	232	72.9	**30.0**	83.2	72.9	109.2	98.8	90.0
	Class 2	101	78.4	48.7	46.0	39.1	36.5	**33.8**	80.9
	Class 3	18	19.2	23.3	**7.0**	34.9	69.4	22.7	19.0
	ALL	114	65.0	38.2	51.3	47.5	67.6	54.4	71.2
	SSC	AFW	EFV_06	TRI_08	PD_200	EFV_MULTI	TRI_MULTI	PD_MULTI	CONF3
VENT 30m	Class 1	245	69.8	95.3	**33.0**	69.8	94.8	**33.0**	85.5
	Class 2	96	47.1	80.8	57.2	**47.1**	64.5	48.6	80.4
	Class 3	63	48.8	63.9	68.9	45.1	**38.3**	76.4	63.9
	ALL	114	**49.8**	69.1	55.8	48.4	54.4	56.9	70.4
	SSC	AFW	EFV_04	TRI_06	PD_280	EFV_MULTI	TRI_MULTI	PD_MULTI	CONF3
SANG 10m	Class 1	122	82.4	**13.8**	85.8	82.4	**13.8**	79.8	94.2
	Class 2	78	18.1	15.8	16.3	17.7	17.1	**13.6**	20.9
	Class 3	22	19.2	17.4	18.3	27.1	**12.8**	29.2	17.4
	ALL	73	32.8	**15.4**	33.1	33.6	15.5	31.9	37.2
	SSC	AFW	EFV_04	TRI_06	PD_240	EFV_MULTI	TRI_MULTI	PD_MULTI	CONF3
SAND 10m	Class 1	53	56.0	84.5	45.7	51.9	48.9	**29.1**	
	Class 2	23	20.3	139.4	43.1	**9.3**	91.8	58.0	
	Class 3	na							
	ALL	41	39.0	106.7	42.2	**37.1**	68.1	39.9	
	SSC	AFW	EFV_06	TRI_06	PD_340	EFV_MULTI	TRI_MULTI	PD_MULTI	CONF3
ESCO 10m	Class 1	160	69.1	**32.2**	70.2	105.3	32.2	56.8	74.0
	Class 2	59	41.4	**37.6**	54.2	143.0	37.6	63.4	47.3
	Class 3	45	50.0	26.3	22.9	49.9	**17.4**	29.7	26.3
	ALL	84	48.7	32.1	51.3	112.6	**31.0**	53.0	49.6
	SSC	AFW	EFV_04	TRI_06	PD_240	EFV_MULTI	TRI_MULTI	PD_MULTI	CONF3
REGI 10m	Class 1	118	63.2	**43.7**	59.2	62.3	53.2	59.4	
	Class 2	79	43.7	50.6	44.9	**35.6**	38.9	39.2	
	Class 3	42	16.4	16.0	13.1	17.7	16.0	12.7	
	ALL	82	45.5	40.2	44.3	42.8	**39.3**	42.4	

Table 3.04 Threshold scores and values for geomorphic valley floor models. Scores in bold are the highest scores in each subwatershed slope class.

		MODEL					
		EFV		TRI		PD	
CARP		Score	Threshold	Score	Threshold	Score	Threshold
MTS	0 to 15	1.446	4	1.554	4	**1.625**	540
	15 to 25	1.488	6	1.354	12	**1.560**	180
	> 25	1.360	6	1.368	8	**1.587**	200
STS	All Sites	1.586	5	**1.590**	**6**	1.504	500
VENT 10-m		Score	Threshold	Score	Threshold	Score	Threshold
MTS	0 to 20	1.635	3	1.585	2	**1.682**	120
	20 to 30	1.530	5	1.549	6	**1.562**	320
	> 30	1.401	6	1.346	10	**1.407**	260
STS	All Sites	1.581	3	**1.5934**	**4**	1.5927	160
VENT 30-m		Score	Threshold	Score	Threshold	Score	Threshold
MTS	0 to 20	1.710	6	1.676	8	**1.778**	200
	20 to 30	1.253	6	**1.517**	14	1.451	280
	> 30	1.457	7	1.331	10	1.399	400
STS	All Sites	1.530	6	1.5392	8	**1.5681**	**200**
SANG		Score	Threshold	Score	Threshold	Score	Threshold
MTS	0 to 20	1.188	4	1.268	6	**1.319**	360
	20 to 30	1.564	4	1.580	4	1.573	160
	> 30	1.326	6	1.487	10	**1.618**	480
STS	All Sites	1.474	4	**1.497**	**6**	1.489	280
SAND		Score	Threshold	Score	Threshold	Score	Threshold
MTS	0 to 15	1.428	3	1.394	4	**1.481**	200
	15 to 25	1.429	5	1.262	4	**1.434**	140
STS	All Sites	**1.476**	**3**	1.454	4	1.464	160
ESCO		Score	Threshold	Score	Threshold	Score	Threshold
MTS	0 to 10	1.520	4	**1.667**	6	1.596	540
	10 to 15	1.358	7	**1.440**	6	1.243	140
	15 to 20	1.493	6	**1.539**	8	1.439	240
STS	All Sites	1.447	6	**1.596**	**6**	1.420	340
REGION		Score	Threshold	Score	Threshold	Score	Threshold
MTS	0 to 15	1.465	4	**1.493**	4	1.411	220
	15 to 25	1.467	5	**1.477**	6	1.443	320
	> 25	1.544	5	1.558	6	**1.595**	240
STS	All Sites	1.489	4	**1.539**	**6**	1.462	240

Validation Sites

During validation, the original seven models and two hybrid models were compared to the remaining field data to select the most accurate models.

The GREM for each of the five pilot watersheds generally performed better than the regional model in terms of overall AAE and RMSE (Tables 3.05 –3.08). Within individual watersheds, the watershed-based models performed better in VENT and SANG, with improved AAE of 7.4 and 6.8 m, respectively (Table 3.07). But the regional model performed better in CARP and ESCO, with improvements in AAE over the watershed-based models of 0.4 m and 2.4 m, respectively. The improvements using the watershed-based models in VENT and SANG were much greater than the losses in accuracy in CARP, and ESCO. In the CARP and ESCO watersheds, the regional models had slightly smaller AAE than the watershed-calibrated models. In the VENT and SANG watersheds, the watershed-calibrated models performed better than the regional model.

Table 3.05. Average absolute errors (AAE) for the geomorphic models during validation. The best performing models for each Subwatershed Slope Class are highlighted with bold text. The best performing models overall are also highlighted with gray fill. AFW = Average field width.

	SSC	AFW	EFV_05	TRI_06	PD_500	EFV_MULTI	TRI_MULTI	PD_MULTI	CONF3	HYB_AAE	HYB_RMSE
CARP 10m	Class 1	144	33.0	18.5	34.0	28.0	**8.0**	35.0	13.0	**8.0**	
	Class 2	18	12.5	**2.5**	36.0	22.5	75.0	10.0	**2.5**	10.0	
	Class 3	28	14.8	17.2	21.5	14.3	11.0	12.3	17.2	13.7	
	ALL	49	18.0	14.5	26.9	18.7	17.4	16.4	13.4	**11.8**	
VENT 10m	SSC	AFW	EFV_03	TRI_04	PD_160	EFV_MULTI	TRI_MULTI	PD_MULTI	CONF3	HYB_AAE	HYB_RMSE
	Class 1	235	93.7	60.4	64.2	93.7	87.0	62.6	72.2	**46.2**	**46.2**
	Class 2	71	26.8	22.1	16.7	25.1	19.7	12.3	27.4	18.7	**12.0**
	Class 3	22	**11.3**	15.4	15.4	30.7	28.7	17.7	12.2	15.4	15.4
	ALL	105	40.3	30.5	29.5	46.0	41.4	28.1	34.8	25.2	**22.6**
VENT 30m	SSC	AFW	EFV_06	TRI_08	PD_200	EFV_MULTI	TRI_MULTI	PD_MULTI	CONF3	HYB_AAE	HYB_RMSE
	Class 1	235	57.6	**31.2**	41.1	57.6	37.2	41.1	43.4	41.1	47.3
	Class 2	31	**2.5**	10.2	24.2	**2.5**	15.5	45.8	10.2	45.8	**2.5**
	Class 3	53	24.5	24.0	24.1	26.6	**17.8**	38.2	25.9	18.3	24.6
	ALL	100	30.0	23.7	28.8	31.2	**22.8**	40.3	28.1	29.2	27.2
SANG 10m	SSC	AFW	EFV_04	TRI_06	PD_280	EFV_MULTI	TRI_MULTI	PD_MULTI	CONF3	HYB_AAE	HYB_RMSE
	Class 1	123	25.0	14.2	41.7	25.0	**10.8**	47.7	29.0	14.2	
	Class 2	50	33.4	**16.0**	24.8	33.2	24.1	32.3	35.0	32.2	
	Class 3	64	29.6	19.3	17.9	**12.7**	15.9	15.5	29.3	15.9	
	ALL	72	30.4	**16.3**	27.9	26.9	19.5	33.1	32.2	24.8	
SAND 10m	SSC	AFW	EFV_04	TRI_06	PD_240	EFV_MULTI	TRI_MULTI	PD_MULTI	CONF3	HYB_AAE	HYB_RMSE
	Class 1	53	176.3	65.0	117.0	175.7	189.7	106.7		65.0	**65.0**
	Class 2	24	**35.3**	105.7	45.3	52.0	87.5	53.3		97.7	52.5
	Class 3	na									
	ALL	34	82.3	99.9	69.2	93.2	121.6	71.1		93.0	**54.3**
ESCO 10m	SSC	AFW	EFV_06	TRI_06	PD_340	EFV_MULTI	TRI_MULTI	PD_MULTI	CONF3	HYB_AAE	HYB_RMSE
	Class 1	220	50.1	**43.6**	74.7	45.8	45.5	82.4	79.8		
	Class 2	76	38.4	**22.7**	52.4	30.3	**22.7**	62.7	40.7		
	Class 3	29	26.2	18.7	26.4	23.5	**5.0**	21.0	20.4		
	ALL	117	38.9	29.5	52.4	34.1	**25.7**	56.5	49.1		
REGION 10m	SSC	AFW	EFV_04	TRI_06	PD_240	EFV_MULTI	TRI_MULTI	PD_MULTI	CONF3	HYB_AAE	HYB_RMSE
	Class 1	135	65.5	**36.8**	68.9	71.4	73.8	69.4		44.6	44.8
	Class 2	71	41.6	51.1	43.0	**38.2**	46.0	44.7		54.5	42.5
	Class 3	30	20.5	17.0	**13.6**	14.0	17.1	13.7		15.0	14.6
	ALL	75	40.5	33.5	39.3	38.7	42.6	40.0		35.8	**31.8**

Table 3.06. Root square mean errors (RSME) for the geomorphic models during validation. The best performing models for each Subwatershed Slope Class are highlighted with bold text. The best performing models overall are also highlighted with gray fill. AFW = average field width.

	SSC	AFW	EFV_05	TRI_06	PD_500	EFV_ MULTI	TRI_ MULTI	PD_ MULTI	CONF3	HYB_ AAE	HYB_ RMSE
CARP 10m	Class 1	144	56.1	26.6	48.2	46.3	**12.1**	49.5	18.6	**12.1**	
	Class 2	18	25.0	**5.0**	52.5	36.4	75.0	15.8	**5.0**	15.8	
	Class 3	28	26.4	27.3	25.8	22.3	**16.3**	21.3	27.3	21.0	
	ALL	49	28.4	22.3	30.5	25.7	28.1	23.5	21.4	**17.0**	
VENT 10m	SSC	AFW	EFV_05	TRI_06	PD_500	EFV_ MULTI	TRI_ MULTI	PD_ MULTI	CONF3	HYB_ AAE	HYB_ RMSE
	Class 1	235	111.7	67.5	75.9	111.7	103.1	77.3	88.8	**52.9**	**52.9**
	Class 2	71	49.4	34.4	22.7	34.4	25.6	18.5	49.5	23.8	**18.1**
	Class 3	22	**18.1**	21.4	20.9	43.2	36.0	28.4	18.9	20.9	20.9
	ALL	105	68.1	43.5	44.8	68.1	61.2	46.0	57.4	34.0	**32.7**
VENT 30m	SSC	AFW	EFV_05	TRI_06	PD_500	EFV_ MULTI	TRI_ MULTI	PD_ MULTI	CONF3	HYB_ AAE	HYB_ RMSE
	Class 1	235	84.7	**42.3**	47.7	84.7	46.0	47.7	61.5	47.7	55.5
	Class 2	31	**4.3**	20.5	36.2	**4.3**	23.7	63.4	20.5	63.4	**4.3**
	Class 3	53	50.8	41.5	38.8	45.5	30.6	46.2	51.1	**27.8**	46.9
	ALL	100	55.2	37.2	38.6	52.8	**32.6**	46.2	48.2	37.6	43.5
SANG 10m	SSC	AFW	EFV_05	TRI_06	PD_500	EFV_ MULTI	TRI_ MULTI	PD_ MULTI	CONF3	HYB_ AAE	HYB_ RMSE
	Class 1	123	32.5	18.3	49.8	32.5	**13.6**	56.3	40.2	18.3	
	Class 2	50	46.5	**20.6**	40.9	46.4	30.6	55.5	50.2	55.3	
	Class 3	64	47.4	31.9	33.3	19.7	23.5	**19.5**	47.3	23.5	
	ALL	72	40.3	**20.9**	39.1	36.9	24.8	47.7	43.9	42.3	
SAND 10m	SSC	AFW	EFV_05	TRI_06	PD_500	EFV_ MULTI	TRI_ MULTI	PD_ MULTI	CONF3	HYB_ AAE	HYB_ RMSE
	Class 1	53	251.7		162.1	250.7	266.3	**146.6**			
	Class 2	24	72.5	151.4	**51.7**	92.3	122.8	60.7		147.9	90.1
	Class 3	na									
	ALL	34	138.3	121.9	90.8	145.0	164.8	87.6		119.2	**74.9**
ESCO 10m	SSC	AFW	EFV_05	TRI_06	PD_500	EFV_ MULTI	TRI_ MULTI	PD_ MULTI	CONF3	HYB_ AAE	HYB_ RMSE
	Class 1	220	70.8	60.2	105.5	**55.8**	60.8	100.0	112.9	60.8	60.8
	Class 2	76	49.4	38.3	81.4	**36.2**	38.3	112.1	79.6	38.3	38.3
	Class 3	29	40.5	30.3	36.5	35.7	**6.9**	29.0	34.4	**6.9**	**6.9**
	ALL	117	53.2	43.5	76.7	42.2	**40.8**	82.1	79.6	**40.8**	**40.8**
REGION 10m	SSC	AFW	EFV_05	TRI_06	PD_500	EFV_ MULTI	TRI_ MULTI	PD_ MULTI	CONF3	HYB_ AAE	HYB_ RMSE
	Class 1	135	89.8	**46.2**	88.6	91.0	96.6	90.1		49.8	50.0
	Class 2	71	54.4	72.7	53.5	**50.8**	62.3	52.0		74.5	55.9
	Class 3	30	31.3	24.6	**19.85**	21.3	24.6	19.86		22.5	21.9
	ALL	75	63.0	53.0	61.7	61.8	67.9	62.0		54.4	**45.8**

Table 3.07 Comparison of minimum AAE error for validations sites for individual watershed versus REGION model for each pilot watershed. Positive values indicate the regional model had smaller errors than the watershed calibrated model.

MODEL TYPE			MINIMUM AAE ERROR Watershed	MINIMUM AAE ERROR Region	W - R*
CARP 10-m	SSC	Class 1	8.0	8.0	0.0
		Class 2	2.5	2.5	0.0
		Class 3	11.0	10.0	1.0
	ALL		11.8	11.4	0.4
VENT 10-m	SSC	Class 1	46.2	39.7	6.5
		Class 2	12.0	50.8	-38.8
		Class 3	11.3	12.5	-1.2
	ALL		22.6	30.1	-7.4
SANG 10-m	SSC	Class 1	10.8	30.0	-19.2
		Class 2	16.0	25.5	-9.5
		Class 3	12.7	14.4	-1.7
	ALL		16.3	23.1	-6.8
ESCO 10-m	SSC	Class 1	43.6	30.3	13.3
		Class 2	22.7	20.7	2.0
		Class 3	5.0		5.0
	ALL		25.7	23.3	2.4

Table 3.08. Summary of selected models for each watershed and REGION

			Constituents by Slope Subclass:										
Pilot H_2Oshed	DEM Used	Selected Model	SSC 1		SSC 2		SSC 3		ERRORS		Model Extent		
			Range	Model	Range	Model	Range	Model	AAE	RMSE	H_2Oshed (km2)	REM (km^2)	% of H_2Oshed
CARP	10-m	HYB-AAE	00 to 15	TRI_LE_04	15 to 25	PD_LE_180	> 25	PD_LE_200	11.8	17.0	40	3	6.3%
VENT	10-m	HYB-RMSE	00 to 20	TRI_LE_04	20 to 30	PD_LE_320	> 30	PD_LE_160	22.6	32.7	585	134	22.9%
VENT	30-m	TRI-MULTI	00 to 20	TRI_LE_08	20 to 30	TRI_LE_14	> 30	TRI_LE_10	22.8	32.6	585	90	15.4%
SANG	10-m	TRI_06	00 to 20	TRI_LE_06	20 to 30	TRI_LE_06	> 30	TRI_LE_06	16.3	20.9	1758	952	54.2%
SAND	10-m	REGION HYB_RMSE	00 to 15	TRI_LE_06	15 to 25	EFV_LE_05	> 25	PD_LE_240	54.3	74.9	393	344	87.5%
ESCO	10-m	TRI_MULTI	00 to 10	TRI_LE_06	10 to 15	TRI_LE_06	> 15	TRI_LE_08	25.7	40.8	221	61	27.6%
REGION	10-m	HYB_RMSE	00 to 15	TRI_LE_06	15 to 25	EFV_LE_05	> 25	PD_LE_240	31.8	45.8	2997	1466	48.9%

Assessing the Benefit of DEM Resolution (10-m versus 30-m) in Geomorphic Boundary Modeling

Analysis of GREM models showed higher accuracy in utilizing 10-m versus 30-m DEMs for model generation. On average the values for 30-m GREM were within 80% of the 10-m GREM. In terms of overall errors, the VENT 10-m GREM and 30-m GREM had an AAE within 0.2 m and RMSE with 0.1 m of each other. Although the overall errors of the 10-m and 30-m GREMs were almost exactly the same, their errors varied within stratified classes (Table 3.12). In SSC1 and SSC3, the 30-m GREM outperformed the 10-m GREM, but in SSC2 the 10-m GREM performed better. A similar trend is exhibited with stream order. Figure 3.02 shows the extents of the best-performing 10-m and 30-m GREM models. The models were HYB_AAE for the 10-m GREM and TRI_MT for the 30-m GREM.

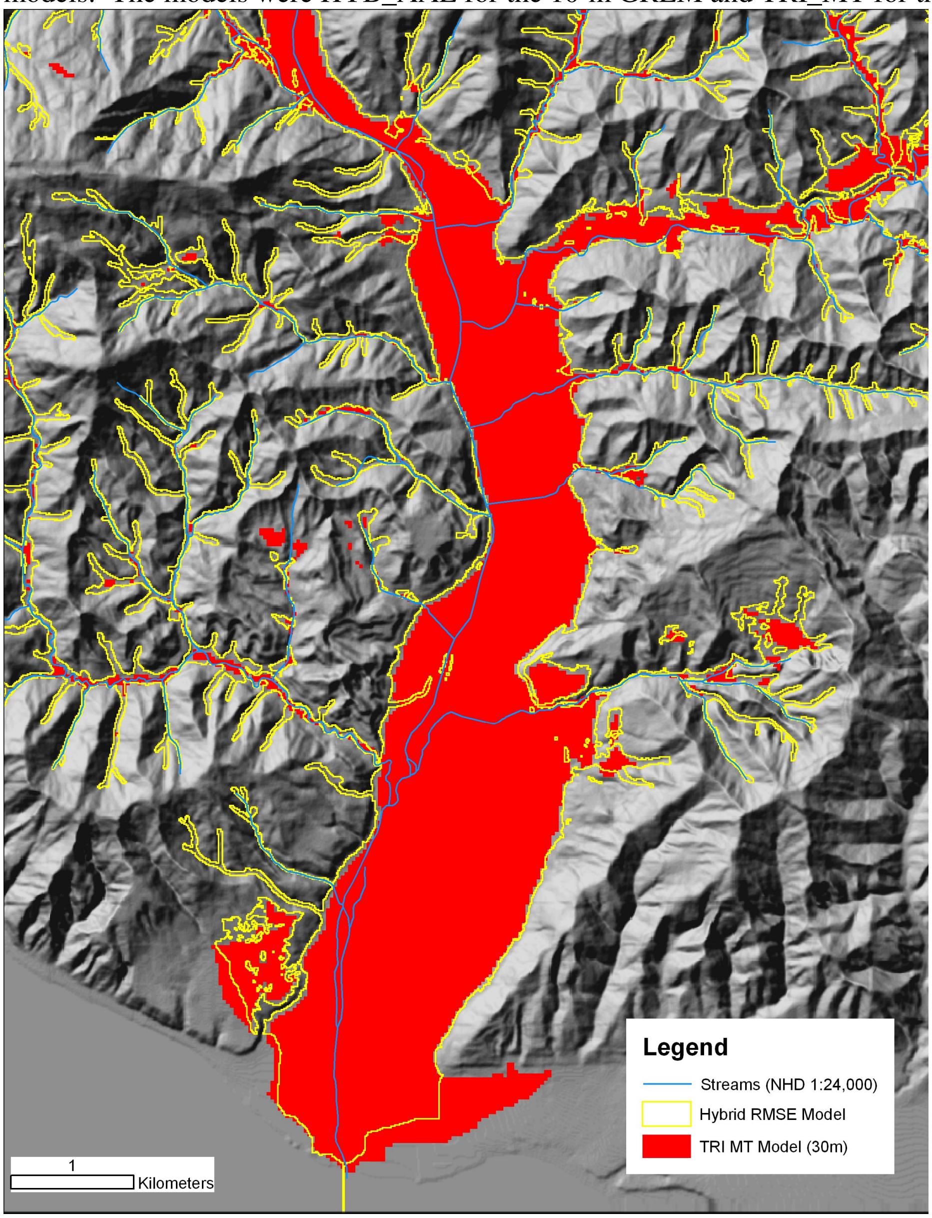

Figure 3.02 Depiction of best performing 10-m and 30-m GREM models.

Table 3.09 Comparison of riparian zone width error for 10- and 30-m GREM. A negative value in the Difference column indicates that the 10-m GREM performed better, while a positive value indicates that the 30-m GREM performed better. FW= Field width. AFW = Average field width.

Validation Sites		#	AFW	10-m GREM (HYB-RMSE)			30-m GREM (TRI_MULTI)			Difference (10-m - 30-m)	
				AMW	AAE	RMSE	AMW	AAE	RMSE	AAE	RMSE
ALL	All	18	100	97	22.6	32.7	86	22.8	32.6	-0.2	0.1
SSC	SSC1 (00-20)	5	235	212	46.2	59.2	213	37.2	46.0	9.0	13.2
	SSC2 (20-30)	7	71	79	12.0	18.1	57	21.8	37.0	-9.8	-19.0
	SSC3 (30-35)	6	22	22	15.4	20.9	15	12.1	16.5	3.3	4.4
FW	< 30-m	8	14	18	8.6	11.6	17	7.9	9.9	0.7	1.6
	> 30-m	10	169	160	33.8	43.7	142	34.8	43.9	-1.0	-0.2
FW	06-15m	5	10	19	10.1	12.4	18	8.4	9.9	1.8	2.5
	15-30-m	3	22	16	6.0	9.2	15	7.0	10.2	-0.9	-0.9
	30-100m	4	44	54	24.5	32.2	25	19.8	26.0	4.6	6.2
	100-200m	3	153	98	55.6	72.9	106	47.6	59.5	7.9	13.5
	200-424m	3	350	364	24.6	41.7	333	41.9	64.2	-17.3	-22.5
Stream Order	2nd to 4th	6	13	17	7.0	10.6	15	6.7	8.6	0.3	2.0
	5th	5	115	110	24.9	37.4	91	31.6	46.9	-6.7	-9.6
	6th to 7th	7	164	156	34.4	44.7	144	30.4	38.4	4.0	6.3

Conversely, the 30-m model performed best at sites where the field-measured valley width was less than 30 m, while the 10-m model performed better at sites greater than 30 m wide. Table 3.10 shows each model's performance in predicting widths at transects less than or equal to 30 m and transects greater than 30 m. A total of 8 validation sites had field widths of less than or equal to 30 m. The 10-m GREM correctly predicted widths of less than 30 m at all 8 of those sites, yielding 100% accuracy for predicting sites with widths less than or equal to 30 m. The 30-m GREM identified 7 out of the 8 sites correctly, yielding 88% accuracy. The 10-m GREM falsely predicted one site to be less than 30 m wide that was actually greater than 30 m.

Table 3.10 Accuracy of 10- versus 30-m DEM in predicting widths at transects with less than30 m or greater than 30 m. "N-field" represents the number of sites based on field width, "Predict N..." represents the number of sites predicted using 10-m or 30-m GREM respectively.

Transect Width	N Field	Predict N 10-m	Accuracy	Predict N 30-m	Accuracy
<= 30-m	8	8	100%	7	88%
> 30-m	10	9	90%	8	80%

With respect to modeled valley edge location. The 10-m DEM model performed with greater accuracy (i.e. lower average errors), but in some cases the 30-m DEM performed better (Table 3.11) .

Table 3.11 Accuracy of modeled valley edge location in VENT watershed using 10-m and 30-m DEM. Positive Difference values reflect that the 10-m DEM performed better(fewer errors) than the 30-m DEM.

STRATIFICATION	CLASS	DEM RESOLUTION				DIFFERENCE
		10-m		30-m		
		#	AAE (m)	#	AAE (m)	
All Sites	na	40	16.3	40	22.0	5.7
Stream Order	2 and 3	2	11.8	7	12.8	1.0
	4	10	14.9	6	14.3	-0.6
	5	11	16.6	10	21.8	5.2
	6	13	17.0	13	29.2	12.2
	7	4	21.6	4	32.4	10.8
SSC	0 - 15	7	19.5	12	32.9	13.4
	15 - 20	6	22.3	10	23.2	0.9
	20 - 30	16	17.8	18	15.6	-2.2
	> 30	11	9.6	0	na	na
Field Width	0-10-m	6	11.8	6	13.7	1.9
	10-25m	7	11.4	7	7.1	-4.3
	25-50m	6	13.6	6	17.1	3.5
	50-100m	5	17.1	5	21.5	4.4
	100-200m	7	22.8	7	31.8	9.0
	>200m	9	20.7	9	40.0	19.3
Category	CAL	19	17.2	19	23.4	6.2
	VAL	18	15.4	18	18.7	3.3
	EX	3	17.0	3	42.0	25.0

Comparison of Approaches for Characterizing Riparian Extent

The Unedited GREM and SSURGO

Comparison of the unedited model using SSURGO indicates that the GREM captured riparian features correctly approximately 86% of the time;14% of the features mapped as riparian could be considered false-positive (Table 3.12).

Table 3.12.Percentage of SSURGO geomorphic features mapped by GREM.

	Geomorphic Description	Total Area (km^2)	Area within GREM (km2)	% of Total Area Mapped by GREM
Non-riparian	badlands	2.8	0.3	9%
	beach	0.3	0.2	49%
	mountains	42.2	8.0	19%
	upland	125.7	15.1	12%
	ALL	171.0	23.5	14%
Riparian	alluvial fan, alluvial	28.8	24.8	86%
	alluvial fan, bench	0.2	0.2	92%
	alluvial fan, terrace	5.6	3.9	70%
	alluvial fan, valley	4.8	4.5	95%
	alluvial plain, basin	0.9	0.4	42%
	drainageway	6.3	5.5	87%
	flood plain	2.2	2.0	95%
	gravel pit	0.2	0.1	56%
	open water	9.9	9.4	94%
	terrace	33.5	28.2	84%
	ALL	92.3	79.0	86%

GREM, NWI and Ferren Riparian Extent Approaches

The 10-m and 30-m GREM for VENT were compared to other approaches or datasets that mapped riparian extent in this watershed. Other approaches/datasets included: 1) the 10-m GREM (HYB_RMSE), 2) 30-m GREM (TRI_MULTI), 3) the NWI wetlands and riparian map, and 4) the Ferren NHD and Ferren DEM maps (generated for this study).

The unedited 10-m GREM approach identified the greatest area at 22.9% of the watershed (Table 3.13). The NWI map and the Ferren approaches had very similar results, ranging from 3.4% to 3.8% of the watershed. The NWI map and the Ferren DEM approach had a total difference in area of only 0.3 km^2.

Table 3.13 Summary of modeled area of riparian zone (RZ) using different models as area and percentage of entire watershed (585 km^2)

Model Type	Model Extent	
	RZ (km2)	% of Watershed
10-m GREM Unedited	134.2	22.9%
10-m GREM Edited	54.9	9.4%
30-m GREM Unedited	90.1	15.4%
NWI Wetland / Riparian	21.7	3.7%
Ferren Buffer NHD	19.8	3.4%
Ferren Buffer DEM Streams	22.0	3.8%

Overall, the 10-m GREM had the lowest AAE and the 30-m GREM had the lowest RMSE with respect to predicted field widths (Table 3.14). In the steepest parts of the watershed (SSC 3), the NWI provided a lower AAE and RMSE than either of the GREM models, with an AAE of 9.8 m and a RSME of 14.2 m, respectively. Overall, the 30-m GREM provided the lowest TAE at 0.1%. Neither of the Ferren models predicted valley width accurately; the Ferren NHD model performed slightly better than the Ferren DEM model.

Table 3.14 Comparison of error in predicting field widths via GREM versus NWI and Ferren et al. (1995) approach.

SSC	10-m GREM		30-m GREM		NWI		Ferren NHD		Ferren DEM	
	AAE	RSME	AAE	RSME	AAE	RSME	AAE	RSME	AAE	RSME
Class 1	46.2	52.9	37.2	46.0	84.4	114.0	165.1	209.8	96.9	126.1
Class 2	12.0	18.1	15.5	23.7	59.6	104.5	16.2	27.2	123.7	181.4
Class 3	15.4	20.9	17.8	30.6	9.8	14.2	48.0	97.3	110.3	155.7
ALL	22.6	32.7	22.8	32.6	49.9	88.0	75.2	124.3	108.8	143.0

In general, the GREM models better predicted valley edge location than the NWI map (Table 3.15). However, with respect to 2nd and 3rd order streams, the steepest sub-watershed slopes (0-m to 10-m valley widths and 10-m to 25-m valley widths) the NWI map performed better. The NWI map also predicted valley edge location more accurately than the GREM models for excluded sites.

Table 3.15 Comparison of the GREM versus NWI in predicting the valley edge location. CAL = calibration, VAL = validation, EX = excluded.

Stratification	Class	Mapping Approach					
		10-m GREM		30-m GREM		NWI	
		#	AAE (m)	#	AAE (m)	#	AAE (m)
All Sites	na	40	16.3	40	22.0	40	24.6
Stream Order	2 and 3	2	11.8	7	12.8	2	6.3
	4	10	14.9	6	14.3	10	15.3
	5	11	16.6	10	21.8	11	23.2
	6	13	17.0	13	29.2	13	30.0
	7	4	21.6	4	32.4	4	63.8
SSC	0 - 15	7	19.5	12	32.9	8	22.6
	15 - 20	6	22.3	10	23.2	5	54.0
	20 - 30	16	17.8	18	15.6	16	27.0
	> 30	11	9.6	0	na	11	9.3
Field Width	0-10-m	6	11.8	6	13.7	6	10.4
	10-25m	7	11.4	7	7.1	7	13.8
	25-50m	6	13.6	6	17.1	7	8.9
	50-100m	5	17.1	5	21.5	6	23.1
	100-200m	7	22.8	7	31.8	6	39.8
	>200m	9	20.7	9	40.0	8	48.2
Category	CAL	19	17.2	19	23.4	19	23.6
	VAL	18	15.4	18	18.7	18	28.2
	EX	3	17.0	3	42.0	4	9.2

Further Comparison of GREM and NWI Approaches

Although the Ferren buffer approach resulted in total riparian areas that were very similar to the NWI map, it had very large valley-width errors in comparison to the GREM and NWI maps. The Ferren multi-width buffer approach was comparable for estimating watershed-scale riparian extent, but not suitable for site or reach-scale mapping. Further comparisons include the GREM and NWI models.

Stream Order and Slope

The 10-m GREM identified roughly three times more areas defined as "riparian" than the NWI map, even after editing the 10-m GREM down from 134.2 km^2 (unedited) to 54.9 km^2 (edited). Further analyses were performed to describe and quantify the differences between the edited 10-m GREM and the NWI map. Tables 3.16-3.18 describe differences of slope and stream order between the edited 10-m GREM and the NWI map.

The 10-m edited GREM mapped a greater proportion of the watershed as riparian areas than NWI, particularly in catchments that contained the lower stream orders (Table 3.16). Nearly 26 km^2 (47%) of the total area of the 10-m edited GREM was allocated to 2nd order streams. By contrast, only 5.8 km^2 (27%) of the NWI extent was allocated to this stream order. The difference in area decreases with increasing stream order. On 7th order streams, the GREM mapped on 32% more area than did NWI.

Table 3.16 Comparison of riparian extent mapped by the 10-m edited GREM versus NWI by stream order, as determined by the Euclidian Allocation process; Section 2.9.2.

Stream Order	Area (km^2)		% of Total Area		Cumulative %		Difference	
	GREM	NWI	GREM	NWI	GREM	NWI	Area (km^2)	GREM / NWI
2nd	25.9	5.8	47%	27%	47%	27%	20.1	449%
3rd	10.1	4.7	18%	22%	66%	48%	5.4	215%
4th	6.9	3.4	13%	16%	78%	64%	3.6	206%
5th	3.9	2.5	7%	11%	85%	75%	1.5	159%
6th	5.7	3.7	10%	17%	96%	92%	2.0	155%
7th	2.3	1.7	4%	8%	100%	100%	0.6	132%
Total Area (km^2)	54.8	21.7						

When represented as slope classes, the GREM and NWI generally mapped a similar percentage of the watershed (Table 3.17), though more total area was identified by the GREM for all but one class (40° to 45°).

Table 3.17 Comparison of riparian extent mapped using the 10-m edited GREM versus NWI according to slope class.

Slope Class	Area (km^2)		% of Total Area		Cumulative %	
	GREM	NWI	GREM	NWI	GREM	NWI
0	6.0	4.2	11%	19%	11%	19%
01 to 10	23.8	9.7	43%	45%	54%	64%
10 to 20	15.7	3.5	29%	16%	83%	81%
20 to 30	7.5	2.5	14%	12%	97%	92%
30 to 40	1.6	1.4	3%	6%	100%	99%
40 to 45	0.2	0.3	0%	1%	100%	100%
Total Area (km^2)	54.8	21.6				

In analyzing the amount of mapped area that overlapped between NWI and the 10-m edited GREM, 14.8 km^2 were mapped by both methods, approximately 68% of the total area mapped by NWI Table 3.18). The GREM mapped an additional 39.9 km^2, more than half of which (22.2 km^2) was allocated to 2nd order streams. Areas mapped only by NWI had higher mean slope values than areas mapped by GREM in all stream orders and agreed areas had lower mean slope values than areas mapped solely by either GREM or NWI in all stream orders.

Table 3.18 Degree of overlap between GREM and NWI riparian extent maps in the VENT watershed. "GREM Only" and "NWI Only" refer to areas that were only mapped by either the GREM or NWI and not captured by the other model. "Agree" refers to areas that were mapped by both methods.

STREAM ORDER	GREM Only		NWI Only		AGREE	
	km^2	Mean Slope	km^2	Mean Slope	km^2	Mean Slope
2nd	22.2	15.5	2.2	18.5	3.6	10.0
3rd	7.1	12.8	1.7	20.1	3.0	8.7
4th	5.0	9.9	1.4	19.2	2.0	8.5
5th	2.4	8.7	0.9	16.3	1.5	7.2
6th	2.4	4.7	0.4	16.9	3.3	2.8
7th	0.8	1.9	0.3	6.7	1.5	1.5
Total Area (km^2)	39.9	13.0	6.9	18.2	14.8	6.8

Stream Length

In general, the 10-m edited GREM had a greater proportion of streamlines mapped within its extent that NWI. The edited GREM had 6% of NHD streamlines outside its mapped riparian extent, while NWI had 30% outside (Table 3.20). Similarly, the edited GREM had 39% of DEM streamlines outside its mapped riparian extent, while NWI 73% outside (Table 3.21). Compared to both the NHD and DEM streamlines, the unedited GREM captures a similar proportion of total stream length, 80% and 81% respectively. However, the edited GREM has very different results. Editing the GREM improves the capture of NHD streamlines to 94%, but falls to only 61% for DEM streamlines. The high inclusion rate of NHD streamlines occurs because the GREM editing process incorporates a 10-m buffer on NHD streamlines to include any streamside riparian extents that were either not captured in the unedited model or were deleted in the initial editing process. The low inclusion rate for DEM streamlines is partially caused by the editing process itself. Large flat areas, such as the Ojai Valley were initially mapped in the GREM, but were edited out because they are primarily orchards. The DEM still modeled streamlines throughout this area, so they were not included in the edited model.

Table 3.19 Comparison length of NHD stream network included in unedited and edited GREM versus NWI riparian map

NHD Stream Network		Unedited GREM			Edited GREM			NWI Map		
Order	Length (km)	Length In (km)	Length Out (km)	% Out	Length In (km)	Length Out (km)	% Out	Length In (km)	Length Out (km)	% Out
1st	582	434	148	25%	547	35	6%	394	189	32%
2nd	184	161	23	12%	173	11	6%	124	61	33%
3rd	83	73	10	12%	75	8	10%	64	19	23%
4th	56	48	8	14%	50	7	12%	43	14	24%
5th	57	54	3	5%	56	1	2%	53	4	7%
Total	963	771	192	20%	901	62	6%	677	286	30%

Table 3.20 Comparison length of DEM stream network included in unedited and edited GREM versus NWI riparian map.

DEM Stream Network		Unedited GREM			Edited GREM			NWI Map		
Stream Order	Length (km)	Length In (km)	Length Out (km)	% Out	Length In (km)	Length Out (km)	% Out	Length In (km)	Length Out (km)	% Out
2nd	630	501	129	21%	377	253	40%	103	527	84%
3rd	310	236	74	24%	179	131	42%	82	228	74%
4th	156	131	25	16%	97	60	38%	61	95	61%
5th	80	70	10	12%	54	26	33%	38	42	52%
6th	52	49	3	5%	43	8	16%	38	14	27%
7th	14	13	1	6%	12	2	11%	11	3	24%

C-CAP Land Cover

Overall, the GREM had more area in each land cover class than did the NWI map (Table 3.22). The largest difference in total area occurred on 2nd and 3rd order streams, where the GREM identified 25.4 km^2 more total area than NWI. 20.3 km^2 of that difference occurred in forest and chaparral / sage land cover classes. The wetland and bare/water class had similar total areas for each model. The forest class had similar total areas in 4th to 7th order areas. All of the other classes had much larger values for the GREM than the NWI map.

Table 3.21. Comparison of C-CAP land cover types occurring within the GREM and NWI mapped riparian extents.

Area (km^2)	Stream Order									All		
	2nd and 3rd			4th and 5th			6th and 7th					
Land Cover Class	GREM	NWI	Δ	GREM	NWI	Δ	GREM	NWI	Δ	GREM	NWI	Δ
Developed	1.4	0.5	0.9	0.9	0.3	0.6	1.4	0.6	0.8	3.7	1.3	2.3
Irrigated Agriculture	0.6	0.2	0.5	0.3	0.1	0.2	0.3	0.1	0.2	1.2	0.4	0.8
Grassland	4.5	1.2	3.3	1.7	0.3	1.4	1.5	0.8	0.7	7.8	2.3	5.5
Forest	13.2	4.2	9.0	3.6	3.0	0.6	0.8	0.6	0.2	17.6	7.8	9.8
Chaparral / Scrub	15.0	3.6	11.3	3.5	1.6	1.9	2.6	2.0	0.6	21.1	7.2	13.9
Wetland	0.9	0.7	0.2	0.8	0.6	0.2	1.3	1.2	0.1	3.0	2.5	0.5
Bare/water	0.2	0.1	0.0	0.0	0.0	0.0	0.2	0.2	0.0	0.3	0.3	0.0
Total	35.8	10.5	25.4	10.8	5.8	5.0	8.0	5.4	2.6	54.6	21.7	32.9

3.4 Comparison of Approaches for Characterizing Riparian Vegetation

The finer-resolution EMERGE data produced an improvement in AAE of predicted canopy Cover of 3.4% (Table 3.23 and Figure 3.03). At validation GPS waypoints with field-measured canopy cover values of 0 to 50%, EMERGE had an accuracy 7.2% better than ETM. At GPS waypoints field-measured canopy cover values of greater than 50%, ETM had accuracy 3.1% better than EMERGE.

Table 3.22. Comparison in accuracies of predicting canopy cover using EMERGE versus ETM data in validation sites.

ALL	Cover Class	#	AAE (in % cover) EMERGE	AAE (in % cover) ETM	Difference (10-m v. 30-m) AAE
		81	20.4	23.8	-3.4
FieldCanopy Cover (0-100%)	0	22	13.0	18.2	-5.3
	01 to 20	18	18.9	24.4	-5.6
	20 to 40	10	9.8	26.9	-17.1
	40 to 60	9	23.0	16.5	6.5
	60 to 80	5	35.2	18.7	16.5
	80 to 100	17	32.2	34.2	-2.0
	100	4	37.0	28.4	8.6

The EMERGE and ETM data generally showed similar predicted canopy cover values as a function of NWI wetland cover classes (Table 3.24). The table shows the NWI wetland types sorted in increasing order by their ETM canopy cover value. The sorting shows a general trend where the marine, lacustrine, estuarine, unconsolidated bottom, unconsolidated shore, and emergent wetland/riparian types exhibit lower mean canopy cover values than scrub-shrub and forested types. Palustrine and riverine scrub-shrub and forested areas comprised 16.6 km^2 or 77% of the total area mapped by NWI.

Table 3.23. Comparison EMERGE and ETM predicted canopy cover values versus NWI.

NWI Attribute				**Mean Canopy Cover %**	
System	Class	Code	Total Area (km^2)	EMERGE	ETM
Palustrine	Unconsolidated Bottom	PUB	0.14	2	9
Riparian	Emergent	RpEM	0.52	8	9
Palustrine	Unconsolidated Shore	PUS	0.04	12	14
Palustrine	Emergent	PEM	0.50	27	26
Riparian	Scrub-Shrub	RpSS	4.22	29	27
Riverine	All	R	3.66	31	32
Palustrine	Scrub-Shrub	PSS	3.46	44	40
Riparian	Forested	RpFO	7.14	68	62
Palustrine	Forested	PFO	1.79	69	62
All	All	All	21.47	47	43

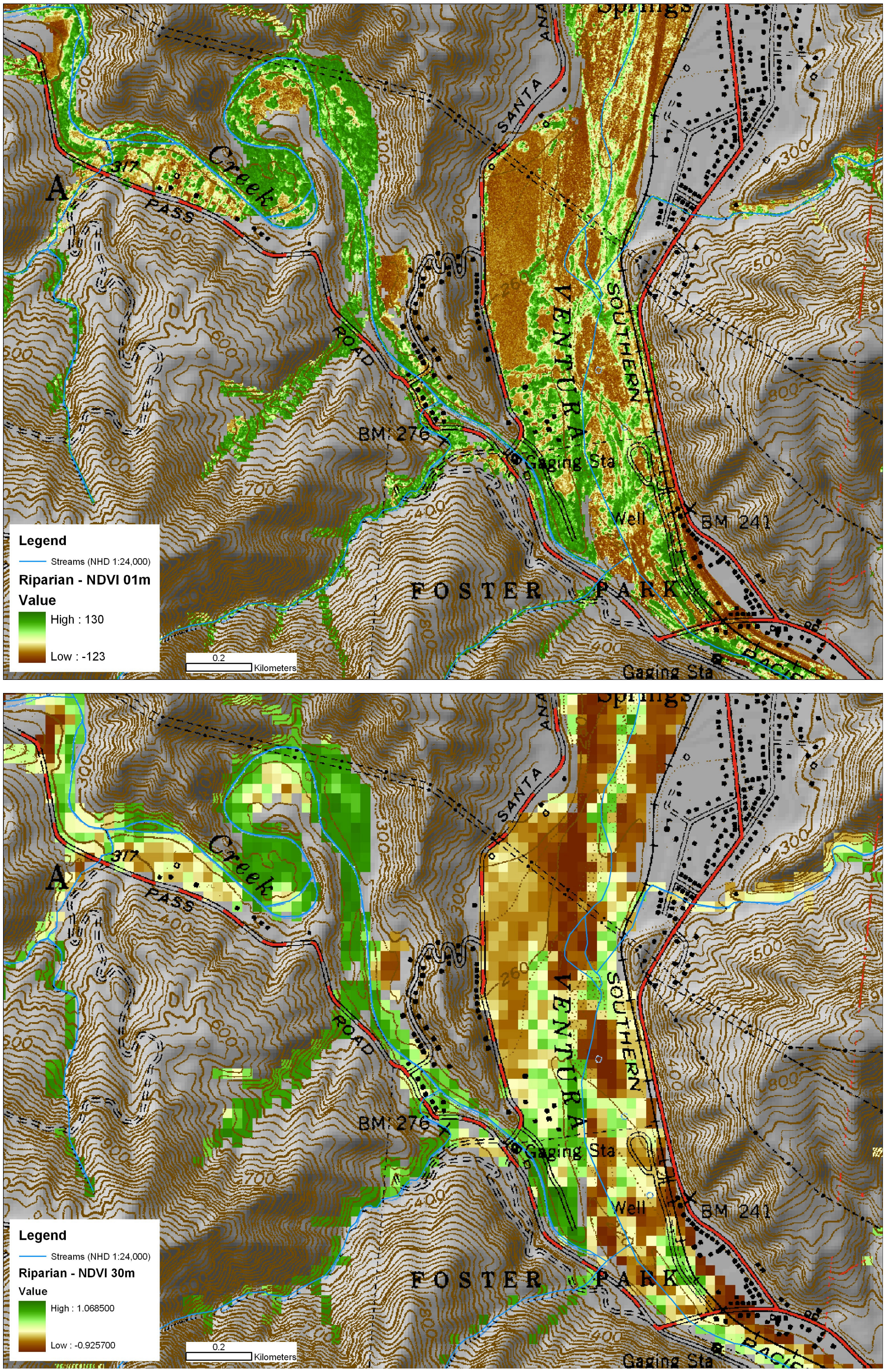

Figure 3.03 Comparison of canopy cover estimates from EMERGE (top panel) and ETM -derived NDVI values (bottom panel).

DISCUSSION

Resource managers and researchers have a variety of needs for riparian maps in order to make sound and effective decisions or observations (Evans et al. 2002). All mapping projects are limited in terms of budgets. Thus, the methodology used to map riparian areas is a function of management needs and the availability of funds for mapping. For mapping to be useful to managers, it must be accurate and provide advantages over traditional approaches; these topics were the focus of this analysis

This study had six major findings:

- A methodology was successfully developed to predict riparian geomorphic extents with the use of either a 10-m or 30-m DEM. The GREM predicted riparian habitat particularly well in areas with high topographic relief or narrow valley walls. It did not take into account the impacts of present-day hydrology on modern riparian habitat and thus had a tendency to overpredict the extent of habitat in wider valleys or in areas, which have been altered by anthropogenic modifications to the floodplain.
- While the 10-m DEM is preferable in terms of reducing modeling errors, a 30-m DEM could be used with acceptable levels of error to predict the geomorphic riparian extent. This is important because for many areas of California, a 10-m DEM is not currently available.
- A regional model was also developed and calibrated based on the physiographic characteristics of the five pilot watersheds. While the customized models for individual watersheds understandably have lower error rates in predicting riparian geomorphic exent, the regional model can be used to predict riparian extent in southern California watersheds without further necessity for fieldwork and model development—thus making the use of this methodology more cost-effective.
- The regional GREM model, in combination with Landsat ETM-derived estimates of vegetative cover, represents a low-cost option for mapping riparian habitat (less than $500 per quad), approximately one- tenth of the cost of mapping riparian habitat using manual interpretation of aerial photography (approximately $5000 per quad).
- High-resolution EMERGE based NDVI (1-m pixel size) only improved accuracy of canopy cover estimation by an AAE of 3.4% over 30-m Landsat ETM data. This marginal improvement in accuracy provided by EMERGE data for this application did not justify the great increase in cost for its acquisition and processing. Because many resource agencies and local conservancies need information not only on vegetative cover but also community or species composition (ie. for invasive species management), those agencies/conservancies with budgets that allow for the acquisition of EMERGE or other high-resolution imagery would most likely use this funding to map riparian vegetative communities with aerial photography or other manual methods.
- Because of the definition of “riparian” employed by the GREM and the way riparian extents are predicted, the delineated habitat represents “potential” or “predicted” habitat. As a result, the GREM + Landsat-derived vegetative cover is more useful as a screening tool to coarsely assess riparian habitat on a regional or statewide scale. Managers who require more detailed and accurate information about the riparian habitat, such as riparian habitat boundaries, regulatory use, local land-use planning, or riparian vegetation composition, and who have available funding will be better served by maps derived from field-based mapping or manual interpretation of aerial photography.

These findings are explained in detail in the next section.

Accuracy of GREM Models in Predicting Riparian Extent

Overall, the accuracy of the GREM in predicting the extent of riverine riparian areas was greatest in areas of high topographic relief. In most watersheds (CARP, VENT, SANG, and ESCO), errors in modeling valley width were positively correlated to the actual valley width (0.95 R^2). The trend did not hold true in SAND, where RMSE was greater than twice the average field-measured width. Figures 2.02 and 2.03 illustrate that more of the SAND watershed was in the lowest slope class and was more developed than any of the other pilot watersheds. These two attributes alone may explain the poor performance of DEM-based riparian extent modeling in SAND. Also the SAND GREM was based on regional threshold values, and therefore had no watershed-based calibration. Detecting rapid topographic changes at the edges of the geomorphic riparian zone can be difficult in subtle topographic settings. Development of the landscape exacerbates this challenge because anthropologic flood control features such as levees and channels are generally not detected in 10-m DEM data. Thus generation of a GREM to map riparian areas in southern California watersheds may require manual correction of the maps in the coastal plains (with ancillary data sets such as FEMA maps), as was conducted for the VENT watershed. Figure 4.01 shows the original and edited HYB-RMSE model for comparison.

While better results may be obtained by collecting field data to customize a model for each individual watershed, it is possible to calibrate one model for use in an ecoregion such as southern California by collecting data in watersheds representing the desired range of physiographic settings. The GREM for each of the five pilot watersheds generally performed better than the regional model in terms of overall AAE and RMSE (Table 3.08). Within individual watersheds, the watershed-based models performed better in VENT and SANG, with improved AAE of 7.4 and 6.8 m, respectively (Table 3.07). However, the regional model performed better in CARP and ESCO, with improvements in AAE over the watershed-based models of 0.4 and 2.4 m, respectively. The improvements using the watershed-based models in VENT and SANG were much greater than the losses in accuracy in CARP, and ESCO. In general the watershed calibration process is therefore beneficial for improving the accuracy of the extent model. Still, it is recognized that the cost-effectiveness of using the GREM to map riparian extent would greatly decrease if necessary to collect field data in order develop a customized GREM in each watershed (Table 4.01). Once a REGION model has been developed for an areasuch as southern California, the model can be run for each watershed at a rate of approximately 5-10 hours ($250-$1000) per watershed, with an additional 5 hours ($250) required for map editing in the lower portion of the floodplain.

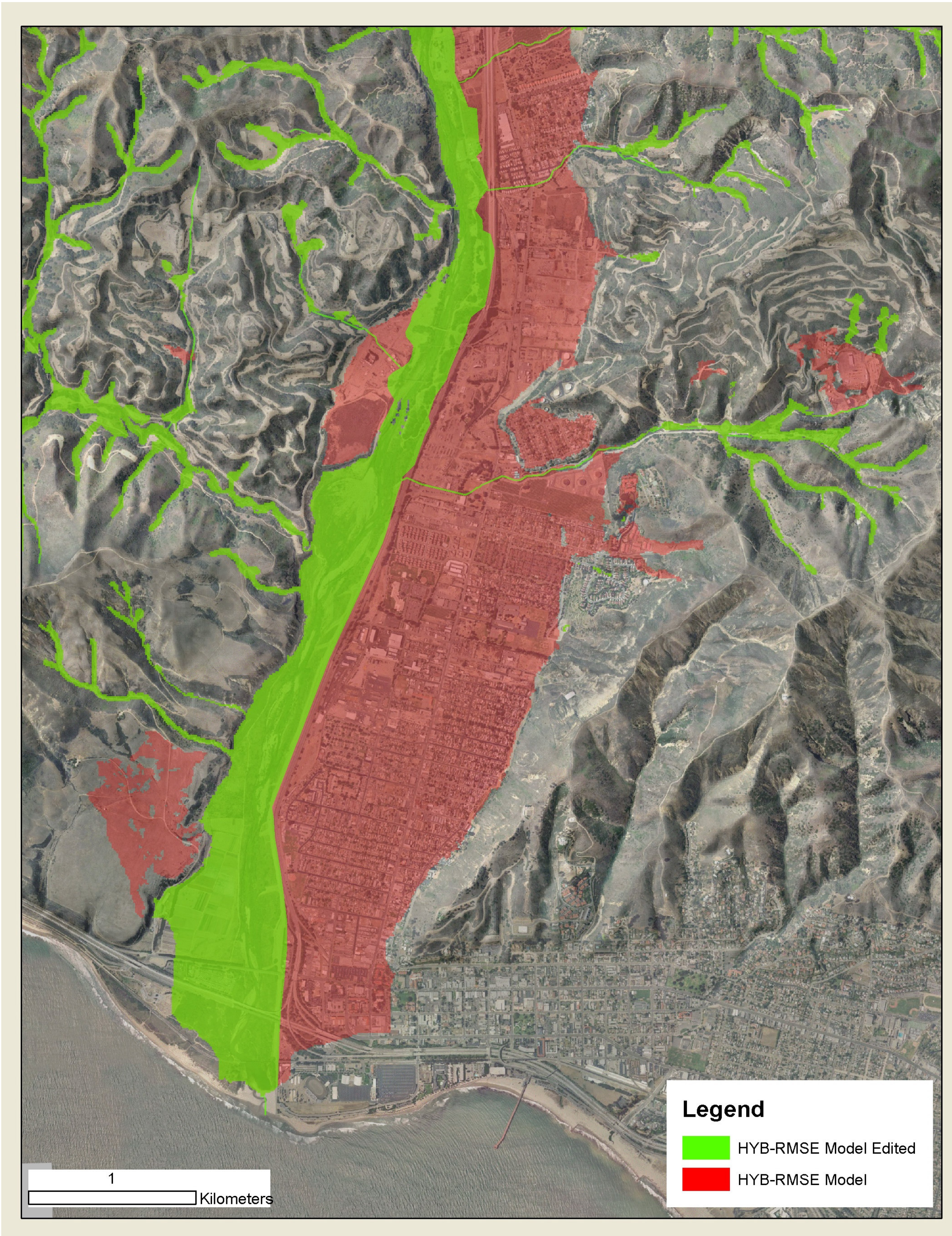

Figure 4.01 Comparison of original (pink) and edited (green) 10-m HYB-RSME model of the modern floodplain in the lower Ventura River

Table 4.01 Summary of numbers of time and associated costs of developing and processing GREM models for each watershed and for the region.

TASK	AMOUNT OF TIME SPENT BY WATERSHED					
Preparation	CARP	VENT	SANG	SAND	ESCO	REGION
Field Reconaisance	5	10	5	10	5	
Site Stratification and ID	5	10	15	5	10	
Landowner Contacts	5	10	5	5	10	
Total	15	30	25	20	25	
Field Data Collection	30	100	30	40	35	
Data Processing						
Field Data	5	40	15	5	10	
DEM, Stream Data	5	15	10	5	5	
Total	10	55	25	10	15	
Model Development						
Threshold Modeling		30				
Riparian Extent Modeling		35				
Model Editing		35				
Total		100				
Model Run						
Threshold Modeling	5	10	10		15	20
Riparian Extent Modeling	5	10	10		20	25
Model Editing		5				
Total	10	25	20	0	35	45
Total Hours	65	310	100	70	110	45
Cost @ $55 per Hour	$3,575	$17,050	$5,500	$3,850	$6,050	$ 2,475

Utility of 10-m versus 30-m DEM in Generating GREM Model

Analysis of GREM models showed higher accuracy in utilizing 10- versus 30-m DEM for model generation. Overall, the VENT 10-m GREM and 30-m GREM had an AAE within 0.2 m and RMSE with 0.1 m of each other. The benefits of using a 10-m relative to a 30-m DEM were most evident in accuracy of locating the edge of the valley. Overall, the AAE for detecting the valley edge location is 16.3 and 22.0 m for the 10-m and 30-m GREM, respectively (Table 3.11). In almost all stratification classes, the 10-m GREM performs best, with a few exceptions. The greatest advantages of using the 10-m GREM for edge location occurred where the valley width was greater than 200 m, on high order streams, and in low SSCs.

Conversely, the 30-m model performed best at sites where the field-measured valley width was less than 30 m, but the 10-m model performed better at sites greater than 30 m wide (Table 3.10). This is a seemingly the reverse of what one would expect. The coarser DEM predicts the width of narrow streams better than the finer DEM. The explanation for this may reside in the rules of the modeling approach. Any segment of stream that is modeled to have a valley width of 0 m is reset to a ½ cell width: 5m or 15 m for the 10-m and 30-m DEMs, respectively. For sites with a field width of less than 30m, the average field width was 14 m. For sites on 2nd to 4th order streams, the average field width was 13 m. For sites in SSC3 the average field width was 22 m. Because the reset value for the 30-m models was 15 m, this closely replicated the actual field widths compared to the 5-m reset value when using the 10-m DEM.

Because the valley edge location may be a more important attribute of the GREM than the modeled valley width, it is clear that it is advantageous to utilize 10-m DEMs rather than 30-m DEMs where possible. The ability of the 10-m GREM to better locate riparian edges means that it is better suited than the 30-m GREM for characterizing site-scale variability. Both the 10m and 30m GREM were found to be equally suited for characterizing the reach-scale variability of valley width.

Comparison of GREM to other Riparian Geomorphic Boundary Models

The GREM model was compared to the Ferren et al. (1995) and the Goetz (2001) method for delineating riparian boundaries in riverine systems. Goetz (2001) reported on a riparian geomorphic boundary model in which a 30-m DEM was used to extract the riparian plain for riparian mapping and inventory purposes. Its strategy differed from the GREM methodology in that it utilized scripts that searched for the location along a stream where the elevation was greater than the elevation of the stream by a specified value. The value for change in elevation was determined by stream order. The script also limited the search for candidate cells to within a specified distance, which also varied per stream order. For example, on 1st order streams, the script would identify all cells within 30-m of the stream, and no higher than 1 ft above the stream cell elevation. On 6th order streams, the script would identify all cells within 600m of the stream, and no higher than 8 ft above the stream cell elevation. Comparison of the RSME for modeled riparian width to field measurements reported by Goetz (2001) versus those of this study indicate that GREM models outperformed the Goetz model (Table 4.02).

Though the Goetz model is innovative in its use of a DEM for riparian boundary delineation, it has some specific limitations. Though the model does not directly use a multi-width buffering scenario, it does impose absolute limits on riparian width based on stream order. The vertical search distance based on stream order also assumes that all riparian areas of a particular stream order have similar geomorphology, which is not always the case. The GREM process uses SSC as a stratifying variable, which may be better associated with riparian width than is stream order.

Comparison of riparian extent mapped via the Ferren et al. (1995) buffer methodology versus the GREM shows that the latter maps a much greater area (Table 3.16). The buffer widths for the Ferren model were based on extensive field sampling with the intention of identifying the amount of riparian areas contributing to the total wetland area of the Ventura River watershed. It is evident that even the edited 10-m GREM predicts a greater area than the Ferren et al (1995) buffer method. The similarity of NWI (3.7% of the watershed) and the Ferren buffers (3.4% and 3.8%) is of interest. It is likely that the visual queues that Ferren et al (1995) used in the field to identify wetlands was similar to the threshold that NWI considered for its riparian mapping. When the Ferren et al (1995) predicted riparian widths are compared to field transects collected for this study, it is clear that the GREM models exhibited fewer overall riparian width errors, assuming Ferren et al (1995) also used the valley edge to define riparian extent (Table 3.17). We cannot discern if the discrepan*cy in mapped riparian extents may be partly or wholly due a difference in the definition used in mapping.*

Table 4.02 Comparison of RMSE for modeled riparian width to field measurements reported by Goetz (2001) versus this study.

MODEL	STREAM ORDER	NUMBER OF SITES	RMSE (METERS)
VENT 10m HYB-RMSE	2 to 4	6	10.6
	5	5	37.4
	6 to 7	7	44.7
	All	18	32.7
VENT 30m TRI-MULTI	2 to 3	3	11.9
	4	4	5.6
	5	4	54.2
	6 to 7	6	42.0
	All	17	32.6
REGION 10m HYB-RMSE	2 to 3	9	28.0
	4	19	41.2
	5	18	47.5
	6 to 8	17	58.1
	All	63	45.8
GOETZ 30m	2	30	58.6
	3	39	69.6
	4	38	43.4
	5	14	70.5
	6	7	105.5
	All	128	69.5

Accuracy and Costs of High- versus Low-resolution Imagery to Map Riparian Vegetative Cover

Currently, manual interpretation of aerial photography is one of the most common, albeit expensive, methods of remotely mapping riparian vegetation communities. In this project, we determined the cost-effectiveness of utilizing high-resolution multi-spectral imagery (EMERGE, 1-m pixel) versus the widely available but low resolution Landsat ETM (30-m pixel) to quantify vegetation cover within the riparian zone. The impetus for this was that it could potentially serve as an alternative means to characterize riparian vegetative if estimates of vegetative cover were sufficient for mapping.

This study found high-resolution EMERGE based NDVI (1-m pixel size) only improved accuracy of canopy cover estimation by an AAE of 3.4% over Landsat ETM data (30-m) (Table 3.25). In this project the 1-meter imagery was too fine to compare to field measurements. First, the recreational grade GPS unit that was used for field data collection had an average positional error of seven meters. The area around a point with a 7-m radius is approximately 70m^2, so an NDVI value from EMERGE imagery would be averaged from approximately 70 pixels. Second, the concave spherical densiometer used to assess canopy cover in the field integrates a varying canopy area, depending on the canopy height above the observer. The field canopy cover measurement was always based on a observation of a canopy area much greater than 1m^2, and perhaps as large as 100m^2 in some cases. Perhaps the use of moderate resolution (and cost) imagery (i.e. IKONOS, SPOT), in combination with higher precision GPS, would yield a better cost/benefit to either EMERGE or Landsat.

he marginal improvement in accuracy provided by EMERGE data for this application does not justify the great increase in cost required for its acquisition and processing (Table 4.03). Furthermore, because many resource agencies and local conservancies need information not only on vegetative cover but also community or species composition (ie. for invasive species management, etc.), those with the budget that would allow the acquisition of EMERGE or other high-resolution imagery would most likely use this funding to map riparian vegetative communities with aerial photography or other manual methods.

Table 4.03 Costs of purchasing and processing EMERGE versus Landsat ETM data for the VENT watershed.

Imagery Type	Acquisition	Processing	Total
Landsat ETM	$400	$550	$950
EMERGE	$18,135	$550	$18,685

Comparison of GREM to Manual Methods of Mapping Riparian Areas

NWI maps of riparian habitat in the VENT watershed, produced by manual interpretation of aerial photography, were compared with the edited 10-m GREM model to determine tradeoffs between accuracy, quality of information provided, and cost.

As with the Ferren et al. (1995) methodology, NWI riparian map of the VENT watershed showed much less area mapped relative to the edited 10-m GREM (Table 3.17). Although GREM models predicted overall riparian zone widths better than NWI data in the VENT watershed, some exceptions to this occurred. First, the NWI map had smaller errors than the GREM models for the steepest slope class (SSC3). Table 3.18 shows a similar trend with respect to detecting the riparian edge location. NWI performed better than GREM in 2nd and 3rd order streams, in areas with a sub-watershed slope of greater than 30 degrees, and at sites with widths of zero to 10 m. NWI also performed better at excluded sites (those with substantial anthropogenic impacts). The reason for the differences between the two methods could be several fold.

First, NWI used a less encompassing definition of riparian habitat than the GREM, where the valley edge definition used in the GREM model. NWI mapped the spectrally distinguishable portions of the landscape, primarily defined by vegetation. GREM mapped topographically low portions of the landscape. One situation where these two differing approaches result in differing boundary delineations occurs when trees at the edge of the geomorphic riparian zone have canopy that extends beyond that geomorphic edge. The vegetative feature actually extends beyond the valley floor from a nadir perspective, contributing to differences in the two maps. Thus, the error exhibited with the NWI data in predicting riparian extent may be partly or wholly due a more restrictive definition of riparian.

Second, because the NWI map is based on current photography, it places the stream and adjacent riparian areas in positions that possibly differ from the DEM/NHD based GREM model. Streams may have meandered since they were mapped for the NHD source (USGS 7.5' quadrangles), or may have been mapped incorrectly originally.

Third, because the NWI map was based on aerial photo interpretation, presumably features that caused sites to be excluded from GREM analysis were detectable and used to map the extent of the riparian area. The GREM method also does not take into account hydrologic regime of the stream and the surrounding floodplain. Thus valley wall definition that is easy to use in this terrain modeling approach includes area that may not typically be considered "riparian" by NWI or other resource management agencies

Finally, all manual methods are subject to human error such as inconsistency of coverage, observer bias and the like. As such, the GREM model could actually help increase the consistency of manual methods of mapping by indicating areas in which riparian habitat is likely to occur and masking out geomorphic uplands. Thus, the GREM methodology may be used in tandem with manual interpretation to increase overall accuracy and consistency of the final product.

It is important to recognize that NWI maps of the VENT watershed not only provide information on riparian extent, but also on the riparian vegetative composition. Thus, manual methods have a distinct advantage of the GREM model in the quality of information that they can provide.

Table 4.04 below provides information on the relative costs of mapping riparian habitat with the GREM + Landsat ETM-derived vegetative cover versus manual methods such as NWI on a per quad basis for the VENT watershed. This shows that if field data and model development must occur to use the model to map riparian extent, the costs are approximately one-half that of manual interpreted aerial photography. However, if a REGION model is already developed, then mapping costs, using the combined GREM+ETM method, are an order of magnitude lower than manually-interpreted aerial photography (<$500 versus $5000 per quad respectively). Note in Table 4.04 that the costs for field data collection and model development in VENT far exceeded the costs for other pilot watersheds. The field and modeling methods were first developed and run for the VENT watershed. Once the methodologies were developed, implementation in new watersheds was much faster and cost efficient. Developing the GREM in VENT cost over $17,000, but the next most expensive watershed was ESCO, with a cost just over $6,000, or approximately $750 per quadrangle.

Table 4.04. Comparison of per quadrangle costs for the 10-m GREM + ETM-derived vegetative cover versus NWI maps in the VENT watershed. Costs are approximate and based on nine quads in the VENT watershed.

METHOD	TOTAL COST	PER QUAD COST	COMMENT
10-m edited HYB-RSME GREM	$17,050	$1,895	Includes cost of field work, model development, and running the model
10-m edited REGION	$2,750	$306	Includes only costs of running the model
Landsat-derived riparian vegetative cover	$1,500	$167	
Manually interpreted aerial photography (NWI in VENT watershed)	$45,000	$5,000	

CONCLUSION

This study successfully developed a methodology to predict riparian geomorphic extents with the use of either a 10-m or 30-m digital elevation model (DEM). This methodology was used to predict riparian extent in 5 pilot watersheds using customized GREM models derived from fieldwork conducted in each watershed. In general, the GREM predicts riparian habitat particularly well in areas with high topographic relief or with narrow valley walls. It does not take into account the impacts of present-day hydrology on modern riparian habitat – and thus has a tendency to overpredict the extent of habitat in wider valleys or in areas, which have been altered by anthropogenic modifications to the floodplain. This study also found that, while the 10-m DEM is preferable in terms of reducing modeling errors, a 30-m DEM could be used with acceptable levels of error to predict the geomorphic riparian extent. This is important because for many areas of California, a 10-m DEM is currently not available. A regional model was also developed and calibrated based on the physiographic characteristics of the 5 pilot watersheds. While the customized models for individual watersheds understandably have lower error rates in predicting riparian geomorphic exent, the regional model can be used to predict riparian extent in watersheds in southern California without further necessity for fieldwork and model development—thus making the use of this methodology more cost-effective.

Comparison of GREM + Landsat mapped riparian habitat versus maps derived from manual interpretation of aerial photography provided a good mechanism for understanding tradeoffs between map accuracy, quality of information provided by the map, and cost. We found that the regional GREM model, in combination with Landsat ETM-derived estimates of vegetative cover, represents a low-cost option for mapping riparian habitat (<$500 per quad), approximately a tenth of the cost of mapping riparian habitat using manual interpretation of aerial photography (approximately $5000 per quad). Use of Landsat ETM (30 m pixel size) versus a higher resolution multi-spectral imagery such as EMERGE (1 m pixel) is preferred in combination with the GREM because the benefit of increased resolution in mapping vegetative cover from EMERGE is greatly outweighed by the increased cost (approximately 18X that of Landsat). Because of the definition of “riparian” employed by the GREM and how riparian extents are predicted, the delineated habitat represents “potential” or “predicted” habitat. As a result, the GREM + Landsat-derived vegetative cover is more useful as a screening tool to coarsely assess riparian habitat on a regional or statewide scale. Managers who require more detailed and accurate information about the riparian habitat (ie riparian habitat boundaries for regulatory use or local land use planning, composition of riparian vegetation) and who have the funding available will be better served by maps derived from field-based mapping or manual interpretation of aerial photography. Towards that end, the GREM model could actually help increase the consistency of manual methods of mapping by indicating areas in which riparian habitat is likely to occur, thus increasing the overall accuracy and consistency of the final product.

LITERATURE CITED

Bendix, J. 1992. Sacle-Related Environmental influences on Southern California Riparian Vegetation, p. 98. The University of Georgia.

Bloom, A. L. 1991. Geomorphology: A Systematic Analysis of Late Cenozoic Landforms, 2nd ed. Prentice-Hall, Inc.

Bren, L. J. 1993. Riparian Zone, Stream, and Floodplain Issues: a Review. Journal of Hydrology 150: 277-299.

Brinson, M.M. (Editor), 1993. Changes in the Functioning of Wetlands Along Environmental Gradients. Wetlands, 13, 65-74 pp.

Brothers, T. S. 1985. Riparian species distributions in relation to stream dynamics, San Gabriel River, California. University of California, Los Angeles.

Cowardin, L. M. C., V.; Golet, F.; Laroe, E.T. 1979. Classification of wetlands and deepwater habitats of the United States. Offices of Biological Services, U.S. Fish and Wildlife Service.

Dahl, T.E., and C.E. Johnson. 1991. Status and trends of wetlands in the conterminous United States: mid-1970's to Mid-1980's. U.S. Department of Interior, Fish and Wildlife Service, Washington, D.C.

DiPietro, D., S. L. Ustin and E. C. Underwood. 2002. Mapping the invasive riparian weed Arundo donax and associated riparian vegetation using AVIRIS. In R. O. Green [ed.], Eleventh JPL Airborne Earth Science Workshop. National Aeronautics and Space Administration.

ESRI, 2005. ArcGIS Desktop Help. http://webhelp.esri.com/arcgisdesktop/9.1/index.cfm?TopicName=welcome

Evans, D., D. Vanderzanden, H. Lachowski, C. Clifton, A. Ager, E. Crowe, J. Hallisey and M. Henstrom. 2002. Stream Geomorphic Classification, Riparian Area Delineation, and Riparian Vegetation Mapping on the Upper Middle Fork of the John Day River, Oregon, p. 18. U.S. Forest Service Remote Sensing Applications Center.

Everitt, J. H., Yang C., Escobar D.E., Lonard R.I., Davis M.R. 2002. Reflectance characteristics and remote sensing of a riparian zone in south Texas. Southwestern Naturalist 47: 433-439.

Ferren, W. R., Jr.; Feidler, P.L.; Leidy, R.A. 1995. Wetlands of the Central and Southern California Coast and Coastal Watersheds.

Ferren, W. R., Jr.; Feidler, P.L.; Leidy, R.A.; Lafferty, K.D.; Mertes, L.A.K. 1996. Wetlands of California, Part II. Description and classification of wetlands of the central and southern coast and coastal watersheds. Madrono 43: 125-182.

Goetz, W. E. 2001. Developing a predictive model for identifying riparian communities at an ecoregion scale in Idaho and Wyoming. p. 74. Geography, Utah State University, Logan.

Goodwin, C. N., C.P. Hawkins and J.L. Kershner. 1997. Riparian Restoration in the Western United States: Overview and Perspective. Restoration Ecology 5: 4-14.

Gregory, S. V. S., F.J.; McKee, W.A.; Cummins, K.W. 1991. An ecosystem perspective of riparian zones. BioScience 41: 540-551.

Harris, R. a. C. O. 1997. Two-Stage System to Prioritize Riparian Restoration at the San Luis Rey River, San Diego County, CA. Restoration Ecology 5: 34-42.

Hemstrom, M., Smith T, Evans D, Clifton C, Crowe E, Aitken M. 2002. Midscale analysis of streamside characteristics in the Upper Grande Ronde Subbasin, Northeastern Oregon, p. 16. USDA Forest Service Pacific Northwest Research Station.

Hewitt, M. J. I. 1990. Synoptic inventory of riparian ecosystems: The utility of Landsat Thematic Mapper data. Forest Ecology and Management 33/34: 605 - 620.

Inlander, E. M. 2002. An integrated methodology for the mapping and inventory of riparian areas of the upper Santa Ynez River watershed, Santa Barbara County, California, p. 223, Geography. University of California Santa Barbara.

Jamieson, B., and D. Braatne. 2001. A comparison of remote sensing tools for assessing the distribution of riparian cottonwood stands in the Colobia Basin, p. 32. BioQuest International Xonsulting Ltd.

Jones and Stokes Associates, I. 1998. Historical riparian habitat conditions of the San Joaquin River - Friant Dam to the Merced River. Prepared for U.S. Bureau of Reclamation, Fresno, California.

Legleiter, C., W. A. Marcus, and R. L. Lawrence. 2002. Effects of Sensor Resolution on Mapping In-Stream Habitats. Photogrammetric Engineering & Remote Sensing 68: 801-807.

Muller, E. 1997. Mapping riparian vegetation along rivers: old concepts and new methods. Aquatic Biology 58: 411-437.

Muller, E., Decampa H, Dobson MK. 1993. Contribution of Space-remote sensing to river studies. Freshwater Biology, 29: 301-312.

Nagler, P., Glenn, EP, Huete, AR. 2001. Assessment of spectral vegetation indices for riparian vegetation in the Colorado River delta, Mexico. Journal of Arid Environments 49: 91-110.

Narumalani, S., Yingchun Zhou, and John R. Jensen. 1996. Application of remote sensing and geographic information systems to the delineation and analysis of riparian buffer zones. Aquatic Biology 58: 393-409.

NSTC 2001.Geomorphometric analysis of surface landscape features. http://www.blm.gov/nstc/ecosysmod/surfland.html

NRC 2002. Riparian Areas: Functions and Strategies for Management. National Academy Press.

NWI. 1998. Project overview. National Wetlands Inventory.

Qi, J., Marsett RC, Moran MS, Goodrich DC, Heilman P, Kerr YH, Dedieu G, Chehbouni A, Zhang XX. 2000. Spatial and temporal dynamics of vegetation in the San Pedro River basin area. Agricultural and Forest Meteorology, 105: 55-68.

Riley, S. J., S. D. DeGloria, and R. Elliot. 1999. A terrain ruggedness index that quantifies topographic heterogeneity. Intermountain Journal of Sciences 5:23-27.

Russell, G. D., C.P. Hawkins, and M.P. O'Neill. 1997. The role of GIS in selecting sites for riparian restoration based on hydrology and land use. Restoration Ecology 5: 56-68.

Strager, J. M., Charles B. Yuill, Petra Bohall Wood. 1997. Landscape-based Riparian Habitat Modeling for Amphibians and Reptiles using ARC/INFO GRID and ArcView GIS. ESRI.

Strahler, A. N. 1957. Quantitative analysis of watershed geomorphology. Transactions of the American Geophysical Union 38: 913-920.

Tiner, R.W., Jr. 1984. Wetlands of the United States: current status and recent trends. U.S. Fish and Wildl Serv. Washington, D.C: U.S. Government Printing Office.

Townsend, P., Walsh, SJ. 2001. Remote sensing of forested wetlands: application of multitemporal and multispectral satellite imagery to determine plant community composition and structure in southeastern USA. Plant Ecology 157: 129-149.

Tucker, C. J. 1979. Red and photographic infrared linear combinations for monitoring vegetation. Remote Sensing of the Environment 8: 127-150.

USDA Forest Service. 2005. FHM Riparian Project. www.fs.fed.us/institute/fhm_riparian/050124_WY_RipInv.ppt

USGS 2006. What is NDVI? http://edc.usgs.gov/greenness/whatndvi.html.

Warner, R. E. a. K. M. Hendrix. 1985. Riparian resources of the Central Valley and California Desert. California Department of Fish and Game, Resources Agency, Sacramento, CA.

Weber, R. M. a. G. A. D. 2001. Riparian Vegetation Mapping and Image Processing Techniques. Photogrammetric Engineering & Remote Sensing 67: 179-186.

WVGAP 2002. A Gap Analysis of West Virginia. West Virginia Gap Analysis Project.